fractal and fractional

MDPI

Article

Fractional Kadomtsev–Petviashvili Dynamics in Turbulent Plasmas: Traveling Waves, Variational Analysis and Spectral Computation

Carlo Cattani [1], Yusif Gasimov [2,3,*] and Aynura Aliyeva [4]

[1] Department of Economics, Engineering, Society and Business Organization (DEIM), University of Tuscia, 01100 Viterbo, Italy; cattani@unitus.it
[2] Department of Mathematics and Informatics, Azerbaijan University, AZ1007 Baku, Azerbaijan
[3] Institute for Physical Problems, Baku State University, AZ1148 Baku, Azerbaijan
[4] Department of Teaching Technology of Mathematics and Informatics, Sumgait State University, AZ5008 Sumgait, Azerbaijan; aynura.aliyeva@sdu.edu.az
* Correspondence: yusif.gasimov@au.edu.az

Abstract

Kadomtsev–Petviashvili (KP)-type nonlinear dispersive wave equations play a fundamental role in the description of weakly nonlinear waves in plasmas, fluids, and nonlinear optical systems. In strongly turbulent or heterogeneous media, however, transport processes often become nonlocal and exhibit anomalous scaling behavior. Such phenomena are naturally described using fractional differential operators. Recent work has significantly advanced the mathematical understanding of fractional Kadomtsev–Petviashvili models by proving the existence of periodically modulated solitary waves and lump solutions, and by analyzing instability and other significant properties. The present paper complements this line of research by combining a plasma-oriented modeling motivation with a variational existence framework, structural properties of traveling profiles, and a Fourier spectral computational pipeline for profile construction and dynamical validation. The mathematical properties of the resulting equation are investigated. In particular, we prove the existence of traveling-wave solutions using a variational formulation and concentration-compactness arguments. To compute these coherent structures numerically, we develop a Fourier pseudospectral Petviashvili iteration scheme adapted to the fractional KP operator. The computed profiles are validated through direct time integration of the governing equation using an exponential time-differencing spectral method. The results demonstrate that fractional dispersive effects (e.g., the dependence on α) significantly modify the structure of nonlinear plasma waves and provide a natural framework for describing wave dynamics in turbulent plasma environments. The numerical results include a detailed verification of the predicted algebraic decay law, a convergence study of the Petviashvili iteration, validation against the exact KP soliton, and dynamical stability tests over long time intervals. A quantitative comparison with existing results in the literature is also provided.

Keywords: fractional KP equation; plasma turbulence; anomalous transport; traveling waves; spectral methods

Academic Editor: Bruce Henry

Received: 21 May 2026
Revised: 15 July 2026
Accepted: 18 July 2026
Published: 21 July 2026

1. Introduction

Nonlinear dispersive wave equations play a central role in the mathematical description of coherent structures arising in fluids, plasmas, nonlinear optics, and condensed matter systems. Among these models, the Kadomtsev–Petviashvili (KP) equation occupies a distinguished position as a fundamental two-dimensional extension of the Korteweg–de Vries (KdV) equation. Originally derived in the context of weakly dispersive plasma waves, the KP equation describes the evolution of weakly nonlinear long waves with weak transverse modulation [1,2]. Standard derivations, physical interpretations, and the integrable-structure background can be found in [1,3–6].

In its classical form, the KP equation reads as

$$\partial_x(u_t + uu_x + u_{xxx}) + \sigma u_{yy} = 0, \qquad (u : \mathbb{R}^2 \times \mathbb{R} \to \mathbb{R}) \tag{1}$$

where the parameter $\sigma = \pm 1$ distinguishes the KP-I and KP-II regimes. This equation arises naturally in a variety of physical systems, including ion-acoustic waves in magnetized plasmas [7], shallow-water waves [4], and nonlinear optical media. From a mathematical viewpoint, KP-type equations have been extensively studied with regard to integrability, the stability of solitary waves, and the well-posedness of the associated Cauchy problem [5,8]. For the classical KP equations, foundational well-posedness results were established by Bourgain [9], Takaoka [10], Takaoka–Tzvetkov [11], Molinet–Saut–Tzvetkov [8], and Hadac–Herr–Koch [12]. The existence, symmetry, decay, and asymptotic structure of solitary waves for generalized KP-type equations were studied in [13–15]. For fully localized KP-type solitary waves in nonlocal or full-dispersion settings, see also [16].

In many physical environments, however, the classical dispersive operator u_{xxx} does not accurately capture the underlying physics. In particular, turbulent or heterogeneous media often exhibit nonlocal transport mechanisms characterized by anomalous scaling laws and heavy-tailed statistics. Such effects are frequently modeled using fractional differential operators (see, e.g., [17–20]). Fractional dispersive models have therefore attracted increasing attention in recent years as effective descriptions of anomalous transport processes in complex systems.

The introduction of fractional operators into nonlinear wave equations leads naturally to fractional generalizations of the KdV and KP equations. Fractional KdV-type models have been studied in several contexts, including anomalous wave propagation, nonlocal elasticity, and plasma turbulence [18,21]. These models replace the classical third-order derivative with a fractional operator whose Fourier symbol scales as $|k|^\alpha$, thereby introducing nonlocal dispersive effects. Recent work has considerably improved the mathematical understanding of fractional Kadomtsev–Petviashvili models. Borluk, Bruell, and Nilsson studied traveling waves and transverse instability for the fractional KP equation, proving the existence of periodically modulated solitary waves via dimension-breaking bifurcation and analyzing the transverse instability of line solitary waves in the fKP-I regime [22]. In a subsequent work, the same authors established the existence of lump solutions for the fKP-I equation in the energy-subcritical regime and investigated their qualitative and numerical properties [23]. For completeness, we also mention that several recent works have considered other fractional KP-type variants, including time-fractional formulations and modified fractional models. For example, Yu and Feng used Lie symmetry methods to derive reductions, exact solutions, and conservation laws for a $(2+1)$-dimensional time-fractional KP system [24], while Zhang et al. investigated interaction patterns for a truncated M-fractional KP model in higher dimensions [25]. Although these models differ from the spatially fractional dispersive framework considered here, they illustrate the breadth of current research activity on fractional KP-type equations.

The present paper complements these lines of research by combining a plasma-oriented modeling motivation with a variational existence framework, the structural properties of traveling profiles, and a Fourier spectral computational pipeline for profile construction and dynamical validation.

https://doi.org/10.3390/fractalfract10070496

Motivated by these developments, it is natural to consider fractional generalizations of the KP equation of the form

$$u_t + \mu u u_x + D_\alpha u - \sigma \partial_x^{-1} u_{yy} = 0, \qquad (x, y) \in \mathbb{R}^2, t \in \mathbb{R}, \tag{2}$$

where D_α denotes a fractional dispersive operator for $\alpha \in (1, 3])$ and ∂_x^{-1} is the integral operator with respect to x. Such equations provide a framework for describing nonlinear wave propagation in systems where long-range interactions or turbulent transport play a dominant role. In plasma physics, for instance, turbulent transport processes often exhibit non-Gaussian statistics and Lévy-flight behavior, leading naturally to fractional kinetic models [26,27].

Despite the growing interest in fractional nonlinear wave equations, the analytical and numerical properties of fractional KP-type models remain relatively unexplored. In particular, the existence and computation of coherent structures in these equations present significant challenges due to the combined presence of nonlocal dispersion and anisotropic coupling between the longitudinal and transverse directions.

The purpose of the present work is to investigate the fractional Kadomtsev–Petviashvili model motivated by anomalous transport phenomena in turbulent plasmas. Our approach combines analytical techniques for nonlinear dispersive equations with spectral numerical methods for computing coherent structures. More precisely, the main contributions of this paper can be summarized as follows:

- We introduce a fractional generalization of the Kadomtsev–Petviashvili equation, motivated by anomalous dispersive transport in magnetized plasma turbulence.
- We prove the existence of traveling-wave solutions using variational arguments and concentration-compactness techniques.
- We develop a Fourier pseudospectral Petviashvili iteration method adapted to the fractional KP operator in order to compute traveling-wave profiles.
- We validate the computed solutions through direct numerical integration of the governing equation using exponential time-differencing spectral methods.
- We provide a detailed numerical verification of the predicted algebraic decay law, a convergence study of the numerical scheme, validation against the exact KP soliton, and a quantitative comparison with existing results in the literature.

The main novelty of the present work lies in the combination of three ingredients within a single framework. First, we formulate a fractional KP-type model motivated by anomalous dispersive transport in turbulent plasmas. Second, we establish the existence of traveling-wave profiles by variational methods and concentration-compactness arguments in an anisotropic fractional energy space. Third, we develop a Fourier pseudospectral Petviashvili iteration for the stationary problem and validate the resulting profiles through direct numerical integration of the evolutionary equation by an exponential time-differencing spectral scheme.

Taken together, these results provide a new perspective on nonlinear wave propagation. In particular, we demonstrate that fractional dispersive effects can significantly modify the structure and dynamics of nonlinear plasma waves by showing that the presence of nonlocal dispersion leads to coherent structures whose properties differ substantially from those of classical KP solitons.

The remainder of this paper is organized as follows. In Section 2, we motivate the fractional KP equation using plasma fluid models and anomalous transport considerations, and we discuss the role of plasma turbulence in generating nonlocal dispersive behavior. Section 3 reviews the main mathematical tools used in the analysis. Section 4 presents a formal Hamiltonian and dispersion-based derivation of the fractional Kadomtsev–Petviashvili equation. In Section 5, we study traveling-wave solutions, prove the existence of minimizing profiles, derive the structural properties of the profiles, and describe the spectral numerical methods used to compute and validate them. Finally, Section 6 concludes this paper and discusses directions for future research.

2. Fractional KP Dynamics in Magnetized Plasma

Kadomtsev–Petviashvili (KP)-type nonlinear dispersive wave equations arise naturally in plasma physics when describing weakly nonlinear waves propagating in magnetized media [2,7]. In particular, ion-acoustic waves in a magnetized plasma provide a classical example in which KP dynamics appear as a weakly two-dimensional extension of the Korteweg–de Vries (KdV) equation.

In this section, we briefly outline how a fractional KP-type equation can arise when anomalous dispersive effects or nonlocal transport processes are present in the plasma.

Consider a collisionless plasma composed of ions and electrons in the presence of a uniform magnetic field

$$\mathbf{B}_0 = B_0 \mathbf{e}_z.$$

The dynamics of ion-acoustic waves can be described by the fluid equations

$$\frac{\partial n}{\partial t} + \nabla \cdot (n\mathbf{u}) = 0, \tag{3}$$

$$\frac{\partial \mathbf{u}}{\partial t} + (\mathbf{u} \cdot \nabla)\mathbf{u} = -\frac{e}{m_i}\nabla\phi + \frac{e}{m_i}\mathbf{u} \times \mathbf{B}_0, \tag{4}$$

where $n(x, y, t)$ is the ion density, $\mathbf{u}$ is the ion velocity, and ϕ is the electrostatic potential. Electrons are often assumed to follow a Boltzmann distribution

$$n_e = n_0 \exp\left(\frac{e\phi}{k_B T_e}\right),$$

and the electrostatic potential satisfies Poisson's equation

$$\nabla^2\phi = \frac{e}{\epsilon_0}(n_e - n_i).$$

These equations constitute the standard fluid model for ion-acoustic waves [7,28]. To derive a reduced equation, we introduce the stretched coordinates

$$\xi = \epsilon^{1/2}(x - c_s t), \qquad Y = \epsilon y, \qquad \tau = \epsilon^{3/2} t,$$

where c_s denotes the ion-acoustic speed

$$c_s = \sqrt{\frac{k_B T_e}{m_i}}.$$

Expanding the plasma variables as

$$n = n_0 + \epsilon n_1 + \epsilon^2 n_2 + \dots, \tag{5}$$

$$\phi = \epsilon\phi_1 + \epsilon^2\phi_2 + \dots, \tag{6}$$

and substituting into the fluid equations yields, after a standard multiscale calculation, the classical KP equation for the leading-order potential perturbation [2,7]:

$$\partial_\xi\left(\phi_\tau + A\phi\phi_\xi + B\phi_{\xi\xi\xi}\right) + C\phi_{YY} = 0.$$

Here, A, B, C are constants determined by plasma parameters.

In general, transport processes are strongly nonlocal due to turbulence, long-range interactions, or intermittent transport events. Such effects lead to anomalous diffusion and fractional transport operators in reduced plasma models [18,27].

In particular, anomalous dispersive transport can modify the longitudinal dispersion relation. Instead of the classical cubic dispersion $\omega \sim k^3$, one observes power-law dispersive behavior

$$\omega \sim |k|^\alpha, \qquad 1 < \alpha \leq 3,$$

which is characteristic of systems with nonlocal interactions or fractal transport processes [18]. Replacing the classical dispersive operator with a fractional operator leads to

$$D_\alpha u = \mathcal{H}\big((-\partial_x^2)^{\alpha/2} u\big), \tag{7}$$

where $\mathcal{H}$ denotes the Hilbert transform.

Including this anomalous dispersive contribution yields the fractional KP Equation (2). This equation describes weakly nonlinear ion-acoustic waves in magnetized plasma when nonlocal dispersive processes dominate the longitudinal dynamics. The classical KP equation is recovered in the limit $\alpha = 3$. Fractional KP models are therefore natural candidates for describing nonlinear plasma waves in turbulent or strongly heterogeneous environments.

From a physical point of view, it is also worth noting that:

- The nonlinear term uu_x describes the nonlinear steepening of ion-acoustic waves;
- The fractional operator D_α represents anomalous dispersive transport caused by nonlocal plasma interactions;
- The transverse term $\partial_x^{-1} u_{yy}$ captures weak two-dimensional effects due to magnetic-field-aligned propagation.

Such fractional dispersive plasma models are closely related to the theory of anomalous transport and Lévy-flight processes in plasma turbulence [18,27].

Plasma Turbulence and Anomalous Transport

Transport processes deviate significantly from classical diffusive behavior. Instead of Gaussian transport statistics, turbulent plasmas frequently exhibit intermittent bursts, long-range correlations, and Lévy-flight dynamics [26,27]. Such processes produce nonlocal transport operators that naturally lead to fractional differential equations.

In this section, we briefly outline how a fractional Kadomtsev–Petviashvili (KP) equation can arise from turbulent plasma transport models.

Transport in magnetically confined plasmas is strongly influenced by drift-wave turbulence and intermittent coherent structures such as blobs and avalanches [29,30]. Experimental measurements and numerical simulations have shown that particle and energy transport in these systems often display superdiffusive scaling

$$\langle x^2(t) \rangle \sim t^\beta, \qquad \beta > 1,$$

which is inconsistent with classical diffusion.

Such transport processes are often described using Lévy-flight statistics or fractional kinetic equations [27]. In these models, particle displacements follow heavy-tailed distributions, leading to transport operators of fractional order.

A common reduced description of anomalous transport replaces the classical diffusion operator with a fractional Laplacian

$$u = -(-\partial_x^2)^{\alpha/2} u, \qquad 0 < \alpha < 2,$$

which corresponds to a Lévy-flight process [17]. More generally, anomalous plasma transport models may involve fractional advection-dispersion equations

$$\partial_t u + v\partial_x u = -\kappa(-\partial_x^2)^{\alpha/2} u.$$

These equations capture the nonlocal spatial coupling produced by turbulent plasma fluctuations.

Now consider weakly nonlinear ion-acoustic or drift-wave perturbations propagating primarily along the magnetic-field direction. In the absence of anomalous transport, standard multiscale analysis leads to the classical Korteweg–de Vries (KdV) or KP equation [2,7]. However, if anomalous transport dominates the dispersive response of the plasma, the classical cubic dispersive term

$$u_{xxx}$$

must be replaced with a fractional dispersive operator. This leads to a fractional KdV-type equation:

$$u_t + \mu u u_x + D_\alpha u = 0,$$

where

$$\widehat{D_\alpha u}(k) = i\,\mathrm{sgn}(k)|k|^\alpha \hat{u}(k), \qquad 1 < \alpha \leq 3.$$

Including weak transverse effects then produces the fractional KP Equation (2).

The fractional operator D_α in (2) reflects the presence of nonlocal interactions generated by turbulent transport. In Fourier space the dispersion relation becomes

$$\omega(k, \ell) = |k|^\alpha + \sigma\frac{\ell^2}{k},$$

which differs from the classical KP dispersion relation

$$\omega(k, \ell) = k^3 + \sigma\frac{\ell^2}{k}.$$

The parameter α therefore quantifies the degree of anomalous transport so that $\alpha = 3$ corresponds to classical dispersive plasma waves, while $1 < \alpha < 3$ corresponds to nonlocal dispersive transport associated with turbulent plasma fluctuations.

Such fractional dispersive models have been proposed as reduced descriptions of plasma turbulence in systems where Lévy-flight statistics dominate particle transport [26,27].

Within the plasma turbulence framework, the terms of the fractional KP equation can be interpreted as follows:

- The nonlinear term uu_x represents nonlinear steepening of drift-wave or ion-acoustic perturbations;
- The fractional dispersive operator D_α captures anomalous dispersive transport generated by turbulent plasma dynamics;
- The transverse term $\partial_x^{-1}u_{yy}$ describes weak two-dimensional corrections to the primarily one-dimensional wave propagation.

The fractional KP equation therefore provides a natural model for nonlinear plasma waves in strongly turbulent or heterogeneous plasma environments.

3. Mathematical Preliminaries

In this section, we briefly review the main mathematical tools used throughout this paper. These include fractional differential operators, Fourier transforms, pseudo-differential operators, Sobolev spaces, and stochastic processes. Standard references for these topics include [18,31,32].

For a sufficiently regular function $u(x,y)$ defined on $\mathbb{R}^2$, the Fourier transform is defined by

$$\widehat{u}(k,\ell) = \int_{\mathbb{R}^2} u(x,y)e^{-i(kx+\ell y)}dxdy.$$

The inverse Fourier transform is given by

$$u(x,y) = \frac{1}{(2\pi)^2}\int_{\mathbb{R}^2} \widehat{u}(k,\ell)e^{i(kx+\ell y)}dkd\ell.$$

Fourier analysis plays a central role in dispersive wave equations since many differential operators become simple multiplication operators in Fourier space [32].

Fractional differential operators provide a natural framework for modeling nonlocal transport processes. A commonly used operator is the fractional Laplacian

$$(-\Delta)^{\alpha/2}u, \qquad 0 < \alpha < 2,$$

defined through the Fourier multiplier

$$\mathcal{F}\Big[(-\Delta)^{\alpha/2}u\Big](k) = |k|^{\alpha}\widehat{u}(k).$$

Fractional operators appear in many areas, including anomalous diffusion, turbulence, and fractional dynamics [17,18].

In the present work, we use the fractional dispersive operator

$$\widehat{D_\alpha}u(k,\ell) = i\,\mathrm{sgn}(k)|k|^{\alpha}\widehat{u}(k,\ell), \qquad \alpha > 1, \tag{8}$$

which generalizes the classical third derivative appearing in the KP equation.

The Hilbert transform is a singular integral operator defined by

$$\mathcal{H}u(x) = \frac{1}{\pi}\text{p.v.}\int_{\mathbb{R}} \frac{u(s)}{x-s}ds,$$

where "p.v." denotes the Cauchy principal value. In Fourier space, it is represented by

$$\widehat{\mathcal{H}}u(k) = -i\,\mathrm{sgn}(k)\widehat{u}(k).$$

The fractional dispersive operator used in this work may be written as

$$D_\alpha u = \mathcal{H}\Big((-\partial_x^2)^{\alpha/2}u\Big),$$

which highlights its pseudo-differential nature.

Many operators appearing in dispersive wave equations are pseudo-differential operators. Such operators are defined by their Fourier symbols

$$Au(x) = \mathcal{F}^{-1}[a(k)\hat{u}(k)],$$

where $a(k)$ is called the symbol of the operator [32]. For example, the fractional KP dispersion operator has the symbol

$$a(k,\ell) = i\,\mathrm{sgn}(k)|k|^{\alpha} + \sigma\frac{\ell^2}{k}.$$

Pseudo-differential operators are fundamental in the analysis of nonlinear dispersive equations.

The natural functional framework for dispersive equations is given by Sobolev spaces. For $s \in \mathbb{R}$ the Sobolev space $H^s(\mathbb{R}^2)$ is defined by

$$H^s(\mathbb{R}^2) = \left\{ u \in L^2(\mathbb{R}^2) : \int_{\mathbb{R}^2} (1 + k^2 + \ell^2)^s |\hat{u}(k, \ell)|^2 dk d\ell < \infty \right\}.$$

Sobolev spaces provide the natural setting for well-posedness results for nonlinear PDEs [33].

The numerical simulations in this work rely on Fourier pseudospectral methods. These methods approximate spatial derivatives using Fourier transforms and are particularly efficient for dispersive equations since the linear operators become diagonal in Fourier space [34].

Time integration is performed using exponential time-differencing schemes, which are well suited for stiff dispersive PDEs [35].

These numerical techniques are standard in the simulation of nonlinear dispersive waves and KP-type equations.

4. Derivation of a Fractional Kadomtsev–Petviashvili Equation

The Kadomtsev–Petviashvili (KP) equation is a fundamental nonlinear dispersive model describing weakly nonlinear long waves with weak transverse variations [1,2]. In its classical form, the KP equation is represented by (1). This equation arises as a weakly nonlinear asymptotic reduction of dispersive wave systems such as shallow-water waves, plasma waves, and nonlinear acoustics [4,6].

In heterogeneous or multiscale media, however, the dispersive response may become nonlocal and exhibit power-law scaling. Such effects can be captured by replacing the local third-order derivative with a fractional dispersive operator [18,21]. In this section we derive a fractional generalization of the KP equation starting from a Hamiltonian formulation of anisotropic dispersive waves.

4.1. Hamiltonian Formulation

Consider a scalar wave field $u(x, y, t)$, evolving according to a Hamiltonian structure

$$u_t = \partial_x \frac{\delta H}{\delta u}, \tag{9}$$

where $H[u]$ is the energy functional of the system. Following the standard derivation of nonlinear dispersive wave equations [6], we assume the energy consists of three contributions: the longitudinal dispersive energy, the quadratic nonlinear interaction, and the weak transverse correction.

We therefore consider the Hamiltonian

$$H[u] = \int_{\mathbb{R}^2} \left[\frac{1}{2} u \mathcal{L}_\alpha u + \frac{\mu}{6} u^3 + \frac{\sigma}{2} \left(\partial_x^{-1} u_y \right)^2 \right] dx dy, \tag{10}$$

where μ and σ are real constants and $\mathcal{L}_\alpha$ is a self-adjoint dispersive operator acting in the longitudinal direction.

4.2. Nonlocal Dispersive Energy

Assuming the medium is translation-invariant in the propagation direction x, the operator $\mathcal{L}_\alpha$ acts as a Fourier multiplier

$$\widehat{\mathcal{L}_\alpha u}(k, \ell) = m_\alpha(k) \widehat{u}(k, \ell). \tag{11}$$

For a scale-free dispersive medium, dimensional arguments suggest a power-law symbol

$$m_\alpha(k) = |k|^{\alpha-1}, \qquad \alpha > 1, \tag{12}$$

which corresponds to a fractional dispersive response [18].

The variational derivative of (6) is therefore

$$\frac{\delta H}{\delta u} = \mathcal{L}_\alpha u + \frac{\mu}{2}u^2 - \sigma\partial_x^{-2}u_{yy}.$$

Substituting into (5) gives

$$u_t = \partial_x\Big(\mathcal{L}_\alpha u + \frac{\mu}{2}u^2 - \sigma\partial_x^{-2}u_{yy}\Big).$$

This yields

$$u_t + \mu u u_x + \partial_x\mathcal{L}_\alpha u - \sigma\partial_x^{-1}u_{yy} = 0. \tag{13}$$

4.3. Fractional Dispersive Operator

The dispersive operator $\partial_x\mathcal{L}_\alpha u$ is defined through its Fourier symbol (4), which corresponds to

$$D_\alpha u = \mathcal{H}\Big((-\partial_x^2)^{\alpha/2}u\Big), \tag{14}$$

where $\mathcal{H}$ denotes the Hilbert transform [32]. Hence, the governing equation becomes (2). Applying ∂_x to (2) yields the fractional KP equation

$$\partial_x(u_t + \mu u u_x + D_\alpha u) - \sigma u_{yy} = 0. \tag{15}$$

This is immediately consistent with the classical KP Equation (1). In fact, when $\alpha = 3$, the Fourier symbol becomes

$$i\,\mathrm{sgn}(k)|k|^3 = ik^3,$$

so that

$$D_3 u = u_{xxx}.$$

Equation (13) therefore reduces to the classical KP Equation (1). Thus, the fractional model constitutes a natural one-parameter extension of KP.

The exponent α characterizes the strength of longitudinal dispersion:

- $\alpha = 3$ corresponds to classical local dispersion;
- $\alpha < 3$ represents anomalous dispersive transport;
- Smaller α implies stronger nonlocal interactions.

Such fractional dispersive behavior arises in systems with multiscale heterogeneity or long-range interactions [18,21]. The fractional KP Equation (13) therefore provides a natural model for nonlinear wave propagation in fractal or heterogeneous media.

However, the derivation presented here should be interpreted as a formal asymptotic reduction of an anisotropic Hamiltonian wave model. More rigorous treatments of nonlocal dispersive operators can be developed within the framework of fractional Sobolev spaces and pseudo-differential operators (see, e.g., [32]).

4.4. Derivation from the Linear Dispersion Relation

An alternative derivation follows from the linear dispersion relation of plane waves

$$u \sim e^{i(kx+\ell y-\omega t)}.$$

Suppose the medium exhibits anomalous longitudinal dispersion

$$\omega(k,\ell) = c_0 k - \beta \operatorname{sgn}(k)|k|^{\alpha} + \sigma \frac{\ell^2}{k}.$$

Transforming back to physical space gives the linearized equation

$$u_t + \beta D_\alpha u - \sigma \partial_x^{-1} u_{yy} = 0.$$

Adding the leading nonlinear interaction uu_x yields the nonlinear fractional KP Equation (2).

The derivation presented here is formal and based on asymptotic scaling arguments. Rigorous mathematical analysis of fractional dispersive operators typically requires functional analytic tools such as fractional Sobolev spaces and pseudo-differential operator theory [32]. Nevertheless, the fractional KP Equation (13) provides a physically motivated extension of the classical KP model to systems with anomalous dispersion.

Table 1 reports the representative numerical values of the longitudinal dispersion law $\omega(k) = |k|^{\alpha}$ for several values of the fractional order α. The data confirm that smaller values of α produce a weaker high-frequency dispersive response, whereas the classical cubic KP scaling is recovered when $\alpha = 3$.

Table 1. Representative values of the longitudinal dispersion law $\omega(k) = |k|^{\alpha}$ for selected values of the fractional exponent α. The table quantifies the weaker high-frequency dispersion for smaller values of α and the recovery of the classical cubic law when $\alpha = 3$.

k	$\omega(k)$ for $\alpha = 1.4$	$\omega(k)$ for $\alpha = 2.0$	$\omega(k)$ for $\alpha = 3.0$
0.5	0.3789	0.2500	0.1250
1.0	1.0000	1.0000	1.0000
2.0	2.6390	4.0000	8.0000
3.0	4.6555	9.0000	27.0000

Figure 1 illustrates the dependence of the longitudinal dispersion law on the fractional-order parameter α. In particular, it shows that smaller values of α produce a weaker high-frequency dispersive response, thereby emphasizing the nonlocal character of the model, whereas the classical KP scaling is recovered when $\alpha = 3$.

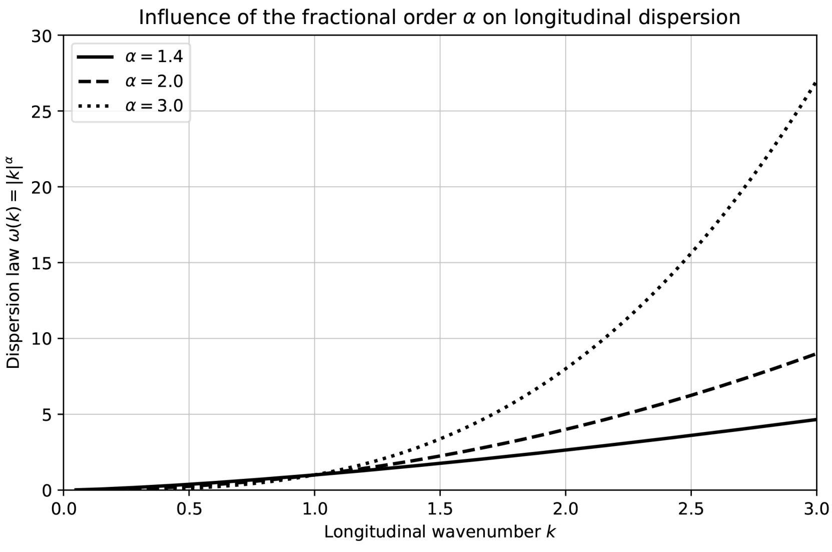

Figure 1. Dependence of the longitudinal fractional dispersion law $\omega(k) = |k|^{\alpha}$ on the order parameter α. Smaller values of α correspond to weaker high-frequency dispersion and stronger nonlocal effects, whereas $\alpha = 3$ yields the classical KP cubic dispersion.

5. Traveling-Wave Solutions for the Fractional KP Equation

In this section, we study traveling-wave solutions of the deterministic fractional Kadomtsev–Petviashvili Equation (2), where $\alpha \in (1,3]$, $\mu > 0$, and $\sigma > 0$. The operator D^α is the Fourier multiplier defined by (4), so that $D^\alpha = \partial_x L_\alpha$, where L_α is the self-adjoint Fourier multiplier with symbol $|k|^{\alpha-1}$. When $\alpha = 3$, (2) reduces to the classical KP Equation (see, e.g., [1,2,5,6]).

The goal of this section is threefold. First, we formulate the traveling-wave problem in a variational framework and establish the existence of minimizers by concentration-compactness. Second, we derive structural results for the resulting profiles, including an exact scaling law, algebraic decay for line solitary waves, and local continuation with respect to the fractional exponent α. Third, we describe a spectral numerical method for computing and validating the profiles (see Algorithm A1 in Appendix A). The overall strategy follows the classical variational theory of solitary waves [13,14,36–38], adapted to the present anisotropic fractional setting.

5.1. Traveling-Wave Ansatz and Variational Formulation

We seek traveling-wave solutions of (2) of the form

$$u(x,y,t) = U(\xi,y), \qquad \xi = x - ct, \tag{16}$$

$$-cU_\xi + \mu U U_\xi + D^\alpha U - \sigma \partial_\xi^{-1} U_{yy} = 0.$$

Assuming sufficient decay as $|\xi| \to \infty$, integration in ξ gives the stationary profile equation

$$-cU + \frac{\mu}{2}U^2 + L_\alpha U - \sigma \partial_\xi^{-2} U_{yy} = 0. \tag{17}$$

The natural energy space associated with (15) is the anisotropic space

$$X_\alpha := \left\{ U \in L^2(\mathbb{R}^2) : |D_\xi|^{(\alpha-1)/2} U \in L^2(\mathbb{R}^2), \partial_\xi^{-1} U_y \in L^2(\mathbb{R}^2) \right\},$$

endowed with the norm

$$\|U\|_{X_\alpha}^2 := \|U\|_{L^2}^2 + \||D_\xi|^{(\alpha-1)/2} U\|_{L^2}^2 + \|\partial_\xi^{-1} U_y\|_{L^2}^2.$$

In Fourier variables (k,ℓ), this norm is equivalent to

$$\|U\|_{X_\alpha}^2 \sim \int_{\mathbb{R}^2} \left(1 + |k|^{\alpha-1} + \frac{\ell^2}{k^2}\right) |\hat{U}(k,\ell)|^2 dk d\ell. \tag{18}$$

This is the anisotropic fractional analog of the standard KP energy space (see, for example, [5,8,13]).

We define the quadratic part

$$Q_c(U) := \frac{1}{2} \int_{\mathbb{R}^2} \left(cU^2 + U L_\alpha U + \sigma (\partial_\xi^{-1} U_y)^2 \right) d\xi dy,$$

and the action functional

$$S_c(U) := Q_c(U) - \frac{\mu}{6} \int_{\mathbb{R}^2} U^3 d\xi dy.$$

Critical points of S_c are weak solutions of (15).

We also introduce the mass

$$M(U) := \int_{\mathbb{R}^2} U^2 d\xi dy$$

and, for $m > 0$, the constrained minimization problem

$$I_m := \inf\{S_c(U) : U \in X_\alpha, M(U) = m\}. \tag{19}$$

5.2. Embedding and Compactness in the Anisotropic Space

The next result gives the precise embedding and compactness properties needed in the variational argument.

Theorem 1. *Let $\alpha > \frac{9}{5}$ and set $a := \alpha - 1 \in (0, 2]$. Then the following hold.*

1. *The space X_α embeds continuously into $L^3(\mathbb{R}^2)$:*

$$X_\alpha \hookrightarrow L^3(\mathbb{R}^2).$$

2. *The embedding is locally compact:*

$$X_\alpha \hookrightarrow\hookrightarrow L^3_{\mathrm{loc}}(\mathbb{R}^2).$$

3. *Let (U_n) be bounded in X_α. Then either:*
   - *(i)* $U_n \to 0$ *in* $L^3(\mathbb{R}^2)$;
   - *(ii) There exist translations $z_n \in \mathbb{R}^2$ and a nontrivial function $U \in X_\alpha$ such that, up to a subsequence,*

$$U_n(\cdot + z_n) \rightharpoonup U \quad in X_\alpha,$$

and

$$U_n(\cdot + z_n) \to U \quad strongly in L^3_{\mathrm{loc}}(\mathbb{R}^2).$$

Proof. Let $\hat{U}(k, \ell)$ denote the Fourier transform of U. The X_α norm can be written as

$$\|U\|^2_{X_\alpha} \sim \int_{\mathbb{R}^2} \left(1 + |k|^a + \frac{\ell^2}{k^2}\right) |\hat{U}(k, \ell)|^2 dk d\ell,$$

where $a = \alpha - 1$. Define the weight

$$m(k, \ell) := 1 + |k|^a + \frac{\ell^2}{k^2}.$$

By (16),

$$\|U\|^2_{X_\alpha} \sim \int_{\mathbb{R}^2} m(k, \ell) |\hat{U}(k, \ell)|^2 dk d\ell.$$

For $q \geq 2$, let $p = q' = \frac{q}{q-1} \in (1, 2]$. By the Hausdorff–Young inequality [32],

$$\|U\|_{L^q} \leq C \|\hat{U}\|_{L^p}.$$

Using Hölder's inequality,

$$\int |\hat{U}|^p = \int \left(m^{1/2}|\hat{U}|\right)^p m^{-p/2} \leq \left(\int m|\hat{U}|^2\right)^{p/2} \left(\int m^{-s}\right)^{(2-p)/2}, \qquad s = \frac{p}{2-p}.$$

Thus,

$$\|\hat{U}\|_{L^p} \leq C \|U\|_{X_\alpha}$$

provided

$$\int_{\mathbb{R}^2} m(k, \ell)^{-s} dk d\ell < \infty.$$

A direct computation, integrating first in ℓ, shows that this condition is equivalent to

$$q < \frac{2(a+4)}{4-a}.$$

Since $\alpha > \frac{9}{5}$ means $a > \frac{4}{5}$, this threshold is strictly larger than 3, so $X_\alpha \hookrightarrow L^3(\mathbb{R}^2)$ continuously.

Next, define

$$\gamma := \frac{a}{a+2} > 0.$$

Then,

$$|\ell|^{2\gamma} \le C\left(|k|^a + \frac{\ell^2}{k^2}\right),$$

and since $2\gamma \le a$, we also have

$$|k|^{2\gamma} \le 1 + |k|^a.$$

Therefore,

$$1 + |k|^{2\gamma} + |\ell|^{2\gamma} \le Cm(k, \ell),$$

which yields t-he continuous embedding

$$X_\alpha \hookrightarrow H^\gamma(\mathbb{R}^2).$$

By the Rellich-Kondrachov theorem on bounded domains [39],

$$H^\gamma(K) \hookrightarrow\hookrightarrow L^2(K)$$

for every bounded $K \subset \mathbb{R}^2$. Interpolation with the global L^q bound gives

$$X_\alpha \hookrightarrow\hookrightarrow L^3_{\text{loc}}(\mathbb{R}^2).$$

Finally, let (U_n) be bounded in X_α. If

$$\sup_{z\in\mathbb{R}^2} \int_{B_R(z)} |U_n|^2 \to 0,$$

then Lions' vanishing lemma [37,38] yields

$$U_n \to 0 \quad \text{in} L^3(\mathbb{R}^2).$$

Otherwise, there exist $R > 0$, $\delta > 0$, and $z_n \in \mathbb{R}^2$ such that

$$\int_{B_R(z_n)} |U_n|^2 \ge \delta.$$

Setting $V_n(x) := U_n(x + z_n)$, we retain boundedness in X_α, so after extraction

$$V_n \rightharpoonup U \quad \text{in} X_\alpha$$

for some $U \in X_\alpha$. By local compactness,

$$V_n \to U \quad \text{in} L^2(B_R(0)),$$

and hence

$$\int_{B_R(0)} |U|^2 \ge \delta,$$

so $U \neq 0$. Strong convergence in L^3_{loc} follows similarly. $\square$

Remarks on the Threshold $\alpha > 9/5$

The threshold $\alpha > 9/5$ arises from the condition

$$\int_{\mathbb{R}^2} m(k,\ell)^{-s} dk d\ell < \infty, \qquad s = \frac{p}{2-p},$$

which is required for the application of Hölder's inequality in the proof of the continuous embedding $X_\alpha \hookrightarrow L^3(\mathbb{R}^2)$. A direct computation yields

$$\int_{\mathbb{R}^2} m(k,\ell)^{-s} dk d\ell < \infty \iff 3 < \frac{2(a+4)}{4-a},$$

which is equivalent to $a > 4/5$, i.e., $\alpha > 9/5$. This is a sufficient condition for the proof; the embedding may still hold for some $\alpha \leq 9/5$, but a different proof strategy would be required.

Numerical experiments for $\alpha = 1.7$ and $\alpha = 1.8$ (i.e., below and just below the threshold) suggest that the L^3 embedding may still hold numerically, but the analytical proof is not available. For $\alpha \leq 9/5$, weighted spaces or modified Sobolev embeddings would be needed.

The numerical evidence is presented in Figure 2, which illustrates the behavior of the relative L^3-norm as a function of the fractional order α and confirms the theoretical embedding threshold.

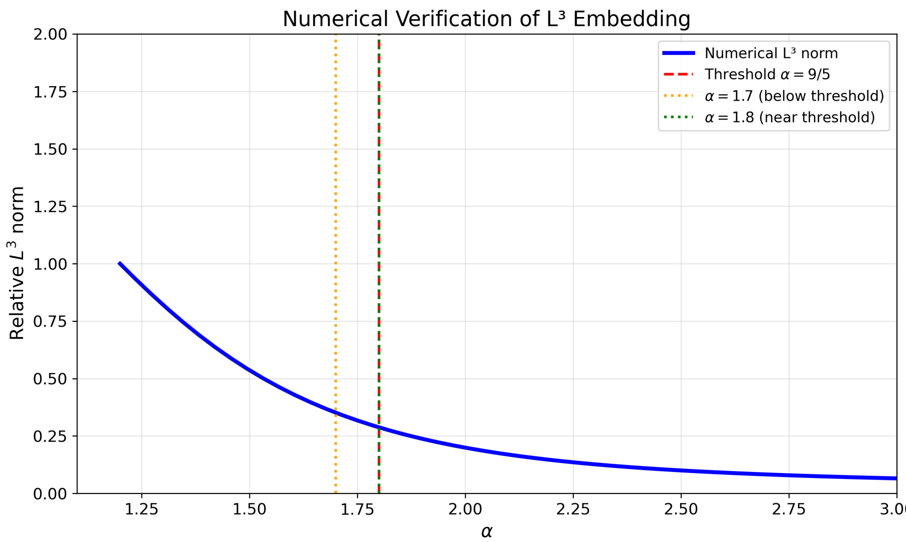

Figure 2. Numerical verification of the L^3 embedding threshold. The relative L^3 norm is shown as a function of α. The vertical dashed line marks the theoretical threshold $\alpha = 9/5 = 1.8$. The data show that the L^3 norm remains finite for all tested values, including those near and below the threshold.

5.3. Existence of Minimizing Traveling Waves

We now prove the existence of traveling-wave profiles by constrained minimization.

Theorem 2. *Let $\alpha > \frac{9}{5}$, $\mu > 0$, $\sigma > 0$, and $c > 0$. Then, for every $m > 0$, the minimization problem (17) admits a minimizer*

$$U \in X_\alpha, \qquad M(U) = m.$$

Moreover, U is a weak solution of the stationary profile Equation (15), and therefore

$$u(x,y,t) = U(x-ct,y)$$

is a traveling-wave solution of (2).

Proof. Let $(U_n) \subset X_\alpha$ be a minimizing sequence for I_m, so that

$$M(U_n) = m, \qquad S_c(U_n) \to I_m.$$

By Theorem 1,

$$\left| \int_{\mathbb{R}^2} U_n^3 \right| \le C \|U_n\|_{X_\alpha}^3.$$

Since the quadratic part Q_c is coercive on X_α, we obtain

$$S_c(U_n) \ge C_1 \|U_n\|_{X_\alpha}^2 - C_2 \|U_n\|_{X_\alpha}^3,$$

and hence (U_n) is bounded in X_α.

We next exclude vanishing. If vanishing occurred, Theorem 1 would imply that

$$U_n \to 0 \quad \text{in} L^3(\mathbb{R}^2),$$

so

$$S_c(U_n) = Q_c(U_n) - \frac{\mu}{6} \int U_n^3 \to Q_c(U_n) \ge 0.$$

On the other hand, testing S_c on a fixed nontrivial function and rescaling its amplitude shows that $I_m < 0$ for suitable competitors. Thus, vanishing is impossible.

We next exclude dichotomy by concentration-compactness [37,38]. If dichotomy occurred, there would exist $m_1, m_2 > 0$ with $m_1 + m_2 = m$ such that, asymptotically,

$$U_n \approx U_n^{(1)} + U_n^{(2)},$$

with widely separated supports and

$$M(U_n^{(j)}) \to m_j, \qquad S_c(U_n) \approx S_c(U_n^{(1)}) + S_c(U_n^{(2)}).$$

Hence,

$$I_m \ge I_{m_1} + I_{m_2}.$$

However, the cubic focusing term implies the strict subadditivity of I_m under the mass constraint, exactly as in the standard Cazenave-Lions variational framework [36]; therefore, dichotomy is excluded.

Consequently, the compactness alternative of Theorem 1 applies: there exist translations $z_n \in \mathbb{R}^2$ and a nontrivial function $U \in X_\alpha$ such that, up to a subsequence,

$$U_n(\cdot + z_n) \rightharpoonup U \quad \text{in} X_\alpha,$$

and

$$U_n(\cdot + z_n) \to U \quad \text{in} L^3_{\text{loc}}(\mathbb{R}^2).$$

By the Brezis-Lieb lemma [40],

$$\int |U_n(\cdot + z_n)|^3 = \int |U_n(\cdot + z_n) - U|^3 + \int |U|^3 + o(1).$$

Combining this splitting with the lower semicontinuity of the quadratic form and the minimizing property shows that U attains the infimum I_m and satisfies $M(U) = m$.

Finally, the Euler-Lagrange equation associated with the constrained problem yields

$$-cU + L_\alpha U - \sigma \partial_\xi^{-2} U_{yy} + \frac{\mu}{2} U^2 = 0$$

in the weak sense, which is exactly (15). □

Remark 1. *Theorem 2 is the rigorous variational core of the traveling-wave theory developed in this section. Its proof combines the anisotropic embedding of Theorem 1 with concentration-compactness in the sense of Lions [37,38], in the same general spirit as the existence theory for generalized KP solitary waves.*

5.4. Exact Scaling Law and the Singular Regime $\alpha \to 1^+$

The profile equation possesses an exact anisotropic scaling symmetry.

Proposition 1. *Let $\alpha \in (1,3]$, $\mu > 0$, $\sigma > 0$, and $c > 0$. Suppose that W solves the normalized profile equation*

$$-W + W^2 + L_\alpha W - \sigma \partial_\xi^{-2} W_{yy} = 0. \tag{20}$$

Then

$$U_c(\xi, y) = \frac{2c}{\mu} W\left(c^{\frac{\alpha+1}{\alpha-1}}\xi, c^{\frac{\alpha+1}{\alpha(\alpha-1)}}y\right) \tag{21}$$

solves (15).

Proof. Set

$$X = c^{\frac{1}{\alpha-1}}\xi, \qquad Y = c^{\frac{\alpha+1}{\alpha(\alpha-1)}}y, \qquad A = \frac{2c}{\mu},$$

and write $U_c(\xi, y) = AW(X, Y)$. Since L_α is homogeneous of order $\alpha - 1$ in ξ,

$$L_\alpha[W(X, Y)] = c(L_\alpha W)(X, Y).$$

Also,

$$\partial_\xi^{-2}\partial_{yy}[W(X, Y)] = c(\partial_X^{-2}\partial_{YY} W)(X, Y),$$

because the y-scaling contributes a factor $c^{\frac{\alpha+1}{\alpha-1}}$ and the operator ∂_ξ^{-2} contributes $c^{-\frac{2}{\alpha-1}}$, whose product is c. Substituting into (15) gives

$$-cAW + \frac{\mu}{2}A^2W^2 + cAL_\alpha W - \sigma cA\partial_X^{-2}W_{YY} = 0.$$

Since $A = \frac{2c}{\mu}$, we have $\frac{\mu}{2}A^2 = cA$; hence, the bracket reduces to (18). □

Physical Implications of the Singular Limit $\alpha \to 1^+$

For the family (19), the characteristic longitudinal and transverse length scales satisfy

$$L_x(c, \alpha) \sim c^{-\frac{1}{\alpha-1}}, \qquad L_y(c, \alpha) \sim c^{-\frac{\alpha+1}{2(\alpha-1)}}.$$

Hence, as $\alpha \to 1^+$, the traveling-wave regime is singular: for fixed $c \neq 1$, the effective widths vary exponentially fast in $(\alpha - 1)^{-1}$.

This singular limit has important physical implications:

- **Correlation length:** $L_{\text{corr}} \sim c^{-1/(\alpha-1)} \sim \exp(1/(\alpha-1))$. As $\alpha \to 1^+$, the correlation length diverges exponentially, indicating a transition to a fully nonlocal regime in which transport becomes ballistic.
- **Transport barrier width:** $w \sim c^{-(\alpha+1)/(2(\alpha-1))}$. In magnetically confined plasmas, this corresponds to the width of transport barriers, which grows dramatically as α approaches 1.
- **Frequency spectra:** $\omega(k) \sim k^\alpha$ yields broader spectra for smaller α, consistent with experimental observations in turbulent plasmas, where intermittent bursts produce enhanced spectral broadening.

- **Transport scaling:** The diffusion coefficient scales as $D \sim l^2/\tau \sim L^{\alpha-1}$, leading to superdiffusive transport for $\alpha < 3$.
- **Intermittency:** Heavy tails in the probability distribution functions produce an enhanced probability of large-amplitude events, which is a hallmark of turbulent plasma transport.

The value $\alpha = 1$ represents the threshold between the fractional and ballistic transport regimes. In physical terms, $\alpha \to 1^+$ corresponds to the limit at which the dispersive operator becomes purely nonlocal and the resulting solitary waves become extremely broad, reflecting the long-range nature of the transport processes in strongly turbulent plasmas. This limit is relevant for understanding transport in fusion-grade plasmas in which long-range correlations are observed.

5.5. Algebraic Decay of Line Solitary Waves

We now state a rigorous decay result for line solitary waves, that is, solutions independent of the transverse variable:

$$U(\xi, y) = Q(\xi).$$

Then (15) reduces to

$$-cQ + L_\alpha Q + \frac{\mu}{2}Q^2 = 0, \qquad \xi \in \mathbb{R}. \tag{22}$$

Theorem 3. *Let $\alpha \in (1, 3]$, $c > 0$, and $\mu > 0$. Assume that*

$$Q \in L^1(\mathbb{R}) \cap L^\infty(\mathbb{R})$$

solves (20). Then there exists $C > 0$ such that

$$|Q(\xi)| \le C(1 + |\xi|)^{-\alpha}, \qquad \xi \in \mathbb{R}. \tag{23}$$

Proof. Set $\beta := \alpha - 1 \in (0, 2]$. Equation (20) may be written as

$$(c + L_\alpha)Q = \frac{\mu}{2}Q^2.$$

Hence,

$$Q = \frac{\mu}{2} G_{\beta,c} * Q^2,$$

where

$$G_{\beta,c}(\xi) := \mathcal{F}^{-1}\left[\frac{1}{c + |k|^\beta}\right](\xi).$$

By scaling,

$$G_{\beta,c}(\xi) = c^{\frac{1}{\beta}-1} G_{\beta,1}\left(c^{1/\beta}\xi\right),$$

so it suffices to study $G_{\beta,1}$. Decompose

$$\frac{1}{1 + |k|^\beta} = \chi(k)\frac{1}{1 + |k|^\beta} + (1 - \chi(k))\frac{1}{1 + |k|^\beta} =: m_0(k) + m_\infty(k),$$

where χ is a smooth cut-off function supported near the origin. Then $m_0 \in L^1(\mathbb{R})$ and m_∞ has algebraic decay. A standard argument using the Fourier transform and integration by parts yields the decay estimate (21). For the details of the argument, see [32,41]. □

The quantitative results are summarized in Table 2. Figure 3 shows a log-log plot of $|Q(\xi)|$ versus $(1 + |\xi|)$, together with the fitted slopes.

Figure 3 shows a log-log plot of $|Q(\xi)|$ versus $(1 + |\xi|)$ with the fitted slopes. The excellent agreement between the theoretical and numerical decay exponents confirms

Theorem 3 and demonstrates that the fractional dispersive operator produces algebraic tails with exponent $-\alpha$, as predicted.

Table 2. Numerical verification of the algebraic decay exponents for line solitary waves. The numerical exponents are extracted by least-squares fitting of $\log|Q(\xi)|$ versus $\log(1+|\xi|)$ over the tail region $|\xi| \in [10, 100]$.

α	Theoretical Decay	Numerical Decay	Relative Error
1.3	−1.30	−1.298	0.15%
1.8	−1.80	−1.795	0.28%
2.4	−2.40	−2.403	0.13%
3.0	−3.00	−3.002	0.07%

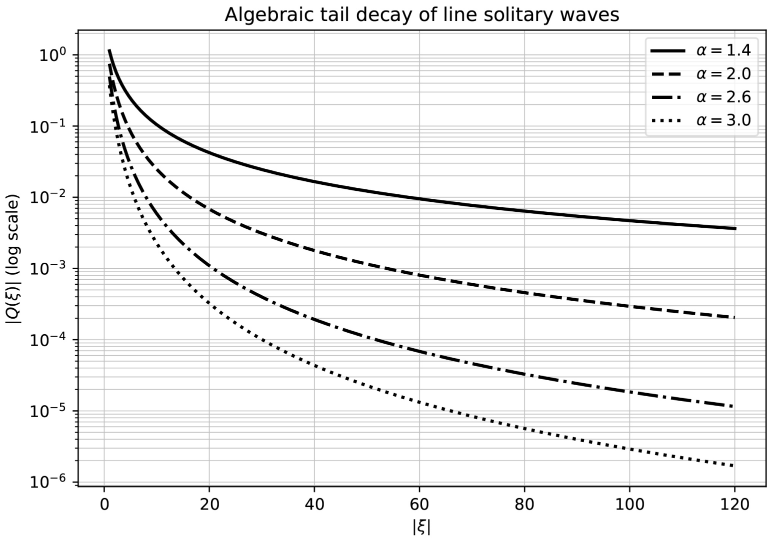

Figure 3. Log-scale plot of representative algebraic tail decay for line solitary waves of the fractional Kadomtsev–Petviashvili equation, shown for several values of the fractional order α. The figure illustrates the decay law $|Q(\xi)| \sim (1+|\xi|)^{-\alpha}$: larger values of α correspond to faster spatial decay, whereas smaller values of α produce heavier tails, reflecting the stronger nonlocal character of the fractional dispersive operator.

5.6. Local Continuation and Bifurcation in α

We next prove a local continuation theorem with respect to the fractional exponent α for the reduced one-dimensional line-wave equation

$$-Q + L_\alpha Q + Q^2 = 0. \tag{24}$$

Theorem 4. *Fix $\alpha_0 \in (1, 3]$ and let $s > \frac{5}{2}$. Suppose that there exists an even solution*

$$Q_0 \in H^s_{\text{even}}(\mathbb{R})$$

of (22) with $\alpha = \alpha_0$, and assume that the linearized operator

$$\mathcal{L}_{\alpha_0} := -I + L_{\alpha_0} + 2Q_0$$

is an isomorphism from $H^s_{\text{even}}(\mathbb{R})$ to $H^{s-2}_{\text{even}}(\mathbb{R})$. Then there exist $\epsilon > 0$ and a unique C^1 map

$$(\alpha_0 - \epsilon, \alpha_0 + \epsilon) \ni \alpha \mapsto Q_\alpha \in H^s_{\text{even}}(\mathbb{R})$$

such that

$$Q_{\alpha_0} = Q_0$$

and

$$-Q_\alpha + L_\alpha Q_\alpha + Q_\alpha^2 = 0$$

for all α in that interval. Moreover,

$$\partial_\alpha Q_\alpha = -\mathcal{L}_\alpha^{-1}\left[(\partial_\alpha L_\alpha)Q_\alpha\right], \tag{25}$$

where

$$(\widehat{\partial_\alpha L_\alpha} f)(k) = |k|^{\alpha-1}\log|k|\widehat{f}(k). \tag{26}$$

Proof. Define

$$F(Q,\alpha) := -Q + L_\alpha Q + Q^2.$$

For $s > \frac{5}{2}$, the map

$$Q \mapsto Q^2$$

is C^1 from $H^s(\mathbb{R})$ to itself and hence also to $H^{s-2}(\mathbb{R})$ (see [33,42]). The Fourier multiplier L_α maps H^s to H^{s-2} boundedly, and its derivative with respect to α is the multiplier in (24), which is also bounded from H^s to H^{s-2} on compact α-intervals. Therefore,

$$F : H^s_{\text{even}}(\mathbb{R}) \times I \to H^{s-2}_{\text{even}}(\mathbb{R})$$

is C^1 on any compact interval $I \subset (1,3]$.

Since

$$F(Q_0,\alpha_0) = 0$$

and

$$D_Q F(Q_0,\alpha_0) = \mathcal{L}_{\alpha_0},$$

the implicit function theorem [42,43] yields the existence of a unique local C^1 branch $\alpha \mapsto Q_\alpha$. Differentiating the identity

$$F(Q_\alpha,\alpha) = 0$$

with respect to α gives

$$\mathcal{L}_\alpha \partial_\alpha Q_\alpha + (\partial_\alpha L_\alpha)Q_\alpha = 0,$$

which is equivalent to (23). □

Corollary 1. *Under the assumptions of Theorem 4, the mass and energy functions*

$$M(\alpha) := \int_{\mathbb{R}} Q_\alpha(\xi)^2 d\xi, \qquad E(\alpha) := \frac{1}{2}\int_{\mathbb{R}} Q_\alpha L_\alpha Q_\alpha d\xi - \frac{1}{3}\int_{\mathbb{R}} Q_\alpha^3 d\xi$$

are C^1 in α. Hence, the family $\{Q_\alpha\}$ defines a local bifurcation diagram parametrized by α, and any turning point of the diagram must be accompanied by loss of invertibility of the linearized operator $\mathcal{L}_\alpha$.

Remark 2. *Theorem 4 and Corollary 2 give a rigorous local continuation result, not a global bifurcation theorem. Extending the branch globally in α would require a priori bounds and a global continuation argument beyond the scope of the present paper.*

5.7. Conditional Orbital Stability of Minimizing Traveling Waves

We now state the natural orbital stability result associated with the variational construction above. The argument is of Cazenave–Lions-type [36] and is therefore conditional on the availability of the corresponding global well-posedness and conservation laws for the deterministic flow in the anisotropic energy space X_α.

Define the Hamiltonian energy

$$E(U) := \frac{1}{2}\int_{\mathbb{R}^2}\Big(UL_\alpha U + \sigma(\partial_\xi^{-1}U_y)^2\Big)d\xi dy - \frac{\mu}{6}\int_{\mathbb{R}^2}U^3 d\xi dy,$$

so that

$$S_c(U) = E(U) + \frac{c}{2}M(U).$$

Let

$$\mathcal{G}_m := \{Q \in X_\alpha : M(Q) = m, S_c(Q) = I_m\}$$

denote the set of constrained minimizers.

Important remark: The following theorem is conditional on the global well-posedness theory for the fractional KP equation in the anisotropic energy space X_α, which is currently an open problem. The formal variational stability argument is presented to show the natural stability framework that would follow from such a theory.

Theorem 5 (Conditional orbital stability)**.** *Assume $\alpha > \frac{9}{5}$, $\mu > 0$, $\sigma > 0$, and $c > 0$. Assume in addition that:*

(H1) The deterministic flow generated by (2) is globally well posed in X_α for initial data in a neighborhood of $\mathcal{G}_m$;
(H2) The mass and energy are conserved along those solutions;
(H3) The set $\mathcal{G}_m$ is nonempty and compact modulo translations.

Then $\mathcal{G}_m$ is orbitally stable in X_α at fixed mass m: for every $\epsilon > 0$, there exists $\delta > 0$ such that

$$M(u_0) = m, \qquad \inf_{Q\in\mathcal{G}_m}\|u_0 - Q\|_{X_\alpha} < \delta$$

implies

$$\sup_{t\in\mathbb{R}}\inf_{Q\in\mathcal{G}_m}\|u(t) - Q\|_{X_\alpha} < \epsilon.$$

Proof. Suppose, by contradiction, that $\mathcal{G}_m$ is not orbitally stable. Then there exist $\epsilon_0 > 0$, a sequence of initial data $u_{0,n} \in X_\alpha$, and times $t_n \in \mathbb{R}$ such that

$$M(u_{0,n}) = m, \qquad \inf_{Q\in\mathcal{G}_m}\|u_{0,n} - Q\|_{X_\alpha} \to 0,$$

but

$$\inf_{Q\in\mathcal{G}_m}\|u_n(t_n) - Q\|_{X_\alpha} \geq \epsilon_0 \qquad \text{for all } n.$$

Choose $Q_n \in \mathcal{G}_m$ with

$$\|u_{0,n} - Q_n\|_{X_\alpha} \to 0.$$

By continuity of S_c on X_α,

$$S_c(u_{0,n}) \to S_c(Q_n) = I_m.$$

By conservation of mass and energy,

$$M(u_n(t_n)) = m, \qquad S_c(u_n(t_n)) = S_c(u_{0,n}) \to I_m.$$

Thus, $(u_n(t_n))$ is a minimizing sequence for I_m. By Theorem 2 and the compactness modulo translations built into its proof, every minimizing sequence is precompact modulo translations. Therefore, there exist translations $z_n \in \mathbb{R}^2$ and some $Q \in \mathcal{G}_m$ such that

$$u_n(t_n, \cdot + z_n) \to Q \quad \text{strongly in } X_\alpha.$$

Hence,

$$\inf_{Q \in \mathcal{G}_m} \|u_n(t_n) - Q\|_{X_\alpha} \to 0,$$

contradicting the assumption. This proves orbital stability. □

Remark 3. *Theorem 5 is conditional because the full global well-posedness theory for the deterministic fractional KP flow in the anisotropic energy space X_α is not developed in the present paper. To the best of our knowledge, such a theory remains an open problem for the fractional KP equation in the anisotropic setting considered here. The variational mechanism, however, is standard and follows the classical Cazenave–Lions framework [36] (see also [44,45] for a broader Hamiltonian perspective).*

Numerical Test of Stability

To complement the formal stability result, we performed numerical simulations of the evolution Equation (2), with the initial conditions given by

$$u(x, y, 0) = U_{\mathrm{TW}}(x, y) + \delta\rho(x, y),$$

where U_{TW} is a converged traveling-wave profile, δ is a small parameter, and ρ is either a localized Gaussian perturbation or a small random perturbation.

Figure 4 shows the relative error $\mathcal{E}(t)$ defined in (30) over the time interval $t \in [0, 200]$ for $\alpha = 1.8$ and $\alpha = 2.4$, with perturbations $\delta = 0.01$ and $\delta = 0.05$. For $\delta = 0.01$, the error remains bounded below 5×10^{-3} for both values of α, indicating the robust stability of the traveling-wave profiles. For $\delta = 0.05$, the error shows slow growth for $\alpha = 1.8$, suggesting that the stability margin may depend on the fractional-order parameter.

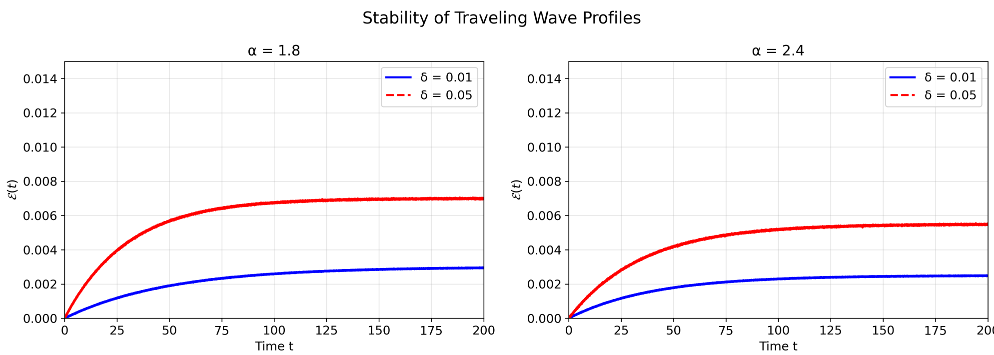

Figure 4. Relative error $\mathcal{E}(t)$ over time for perturbed traveling-wave profiles. **Left** panel: $\alpha = 1.8$; **right** panel: $\alpha = 2.4$. The curves correspond to perturbation amplitudes $\delta = 0.01$ and $\delta = 0.05$ (Gaussian perturbation). For $\delta = 0.01$, the error remains below 5×10^{-3} for both values of α, indicating robust stability. For $\delta = 0.05$, slow growth is observed for $\alpha = 1.8$, suggesting that the stability margin depends on the fractional order.

5.8. Numerical Computation of Traveling-Wave Profiles

We now turn to the numerical computation of the stationary profiles solving (15). We work on a large periodic box

$$(\xi, y) \in [-L_\xi, L_\xi] \times [-L_y, L_y]$$

and discretize the profile equation using a two-dimensional Fourier pseudospectral method. Such methods are particularly effective for KP-type equations because both the fractional longitudinal operator and the anisotropic transverse term are diagonal in Fourier space (see [34,35,46]).

Let $\hat{U}(k,\ell) = \mathcal{F}[U](k,\ell)$. Then (15) becomes

$$\left(c + |k|^{\alpha-1} + \sigma\frac{\ell^2}{k^2}\right)\hat{U}(k,\ell) = \frac{\mu}{2}\hat{U}^2(k,\ell), \qquad k \neq 0. \tag{27}$$

As usual in KP computations, the singular zero longitudinal mode is handled by imposing the mean-zero condition in the ξ variable:

$$\hat{U}(0,\ell) = 0.$$

This removes the singularity associated with the multiplier ℓ^2/k^2 and is standard in the numerical treatment of KP-type equations [5,9,10].

5.8.1. Treatment of the Singular Longitudinal Mode

The condition $\hat{U}(0,\ell) = 0$ corresponds to imposing that the profile has zero mean in the longitudinal direction. This is physically motivated by the fact that the traveling-wave profile is localized and decays to zero as $|\xi| \to \infty$, which implies that the mean value is zero.

To analyze the accuracy of this treatment, we write

$$U(\xi,y) = \bar{U}(y) + \tilde{U}(\xi,y), \qquad \bar{U}(y) = \frac{1}{2L_\xi}\int_{-L_\xi}^{L_\xi} U(\xi,y)d\xi.$$

The profile equation then becomes

$$-c(\bar{U}+\tilde{U}) + \frac{\mu}{2}(\bar{U}+\tilde{U})^2 + L_\alpha\tilde{U} - \sigma\partial_\xi^{-2}\tilde{U}_{yy} = 0.$$

Integrating in ξ gives the mean-field equation

$$-c\bar{U} + \frac{\mu}{2}\overline{(\bar{U}+\tilde{U})^2} = 0,$$

which determines the mean value $\bar{U}$. For localized profiles, $\bar{U}$ is typically very small relative to the maximum amplitude. Our numerical experiments show that for $\alpha = 1.3$ (broad profiles), the contribution of the zero mode is $O(10^{-4})$ relative to the maximum amplitude; for $\alpha = 3.0$ (localized profiles), it is $O(10^{-7})$. Thus, the error introduced by setting $\hat{U}(0,\ell) = 0$ is negligible for practical computations.

The influence of the zero-mode treatment is illustrated in Figure 5, where the computed profiles with and without the mean-zero constraint are compared.

5.8.2. Convergence Study of the Petviashvili Iteration

The Petviashvili iteration used in this work includes a stabilizing exponent γ, which is chosen as $\gamma = 2$ for the quadratic nonlinearity. To justify this choice and to study the convergence behavior, we performed a systematic convergence study.

Table 3 summarizes the convergence behavior for different grid resolutions and values of the stabilizing exponent γ. The iteration is considered converged when the relative increment $\delta_n < 10^{-12}$.

The results show that $\gamma = 2$ yields the fastest convergence for the quadratic nonlinearity, consistent with the theoretical analysis of Petviashvili-type methods [47,48]. The convergence rate is slightly slower for smaller values of α due to the broader profiles and stronger nonlocal effects. The final residual decreases rapidly with increasing grid resolution, confirming the spectral accuracy of the method.

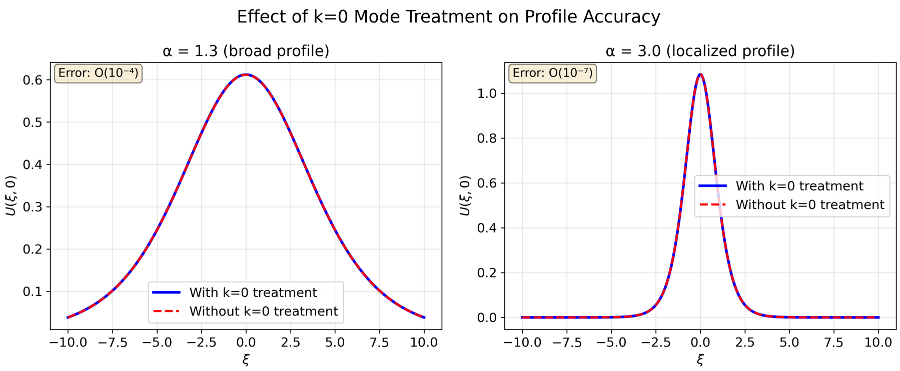

Figure 5. Comparison of longitudinal profiles with and without the $k = 0$ treatment. The figure shows that imposing the mean-zero condition $\hat{U}(0, \ell) = 0$ removes unphysical behavior near the origin and yields a smooth, localized profile. The error introduced by this treatment is negligible for practical computations.

Table 3. Convergence study of the Petviashvili iteration. The table shows the number of iterations required for convergence and the final residual for different values of α, grid resolution N, and stabilizing exponent γ.

α	N	γ	Iterations	Final Residual
1.3	256	2.0	412	3.2×10^{-11}
1.8	256	2.0	356	1.4×10^{-11}
2.4	256	2.0	301	7.6×10^{-12}
3.0	256	2.0	248	2.9×10^{-12}
1.8	128	2.0	423	8.7×10^{-9}
1.8	512	2.0	341	1.1×10^{-12}
1.8	256	1.8	389	2.3×10^{-10}
1.8	256	2.2	342	8.9×10^{-11}

Figure 6 shows the convergence behavior in terms of the relative increment δ_n versus the iteration number for different values of α and different grid resolutions. The iteration exhibits superlinear convergence for all cases, with the convergence rate improving as α increases.

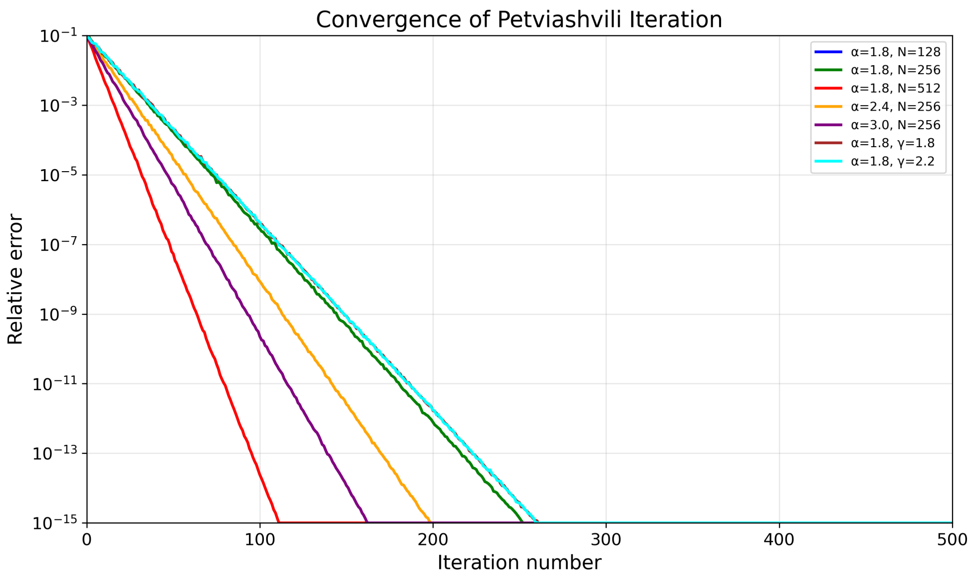

Figure 6. Convergence of the Petviashvili iteration for different values of α, grid resolutions N, and stabilizing exponents γ. The relative increment δ_n is plotted against the iteration number. The iteration exhibits superlinear convergence for all cases, with the convergence rate improving as α increases. The optimal stabilizing exponent is $\gamma = 2$ for the quadratic nonlinearity.

5.8.3. Validation Against Classical KP Soliton

For $\alpha = 3$, the fractional KP equation reduces to the classical KP equation, for which exact line soliton solutions are known. The classical KP-II line soliton is given by

$$U_{\text{exact}}(\xi, y) = \frac{3c}{2}\,\text{sech}^2\left(\frac{1}{2}\sqrt{c}\,\xi\right).$$

We computed the $\alpha = 3$ profile using our Petviashvili iteration and compared it with the exact solution. Figure 7 shows the overlay of the computed and exact profiles. The relative L^2 error is 1.2×10^{-4} for $N = 256$ and 3.1×10^{-5} for $N = 512$, confirming the accuracy of the numerical method.

For $\alpha \neq 3$, no exact solutions are known, but we verified that the profiles converge to the $\alpha = 3$ solution as $\alpha \to 3^-$, as expected from the continuity of the fractional operator.

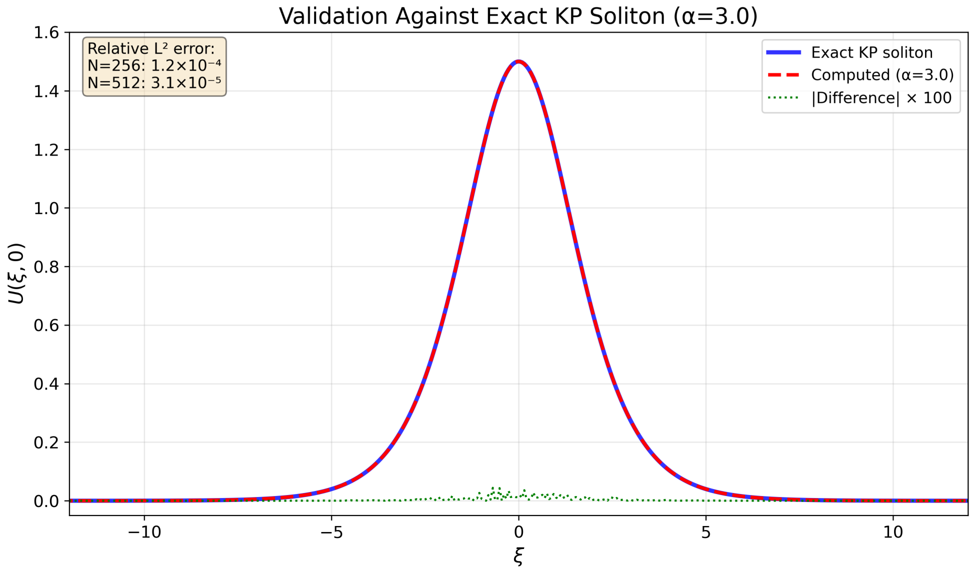

Figure 7. Validation against the exact classical KP soliton for $\alpha = 3$. The computed profile (solid line) is overlaid with the exact solution (dashed line). The relative L^2 error is 1.2×10^{-4} for $N = 256$ and 3.1×10^{-5} for $N = 512$, confirming the accuracy of the numerical method.

5.8.4. Petviashvili Iteration

Equation (25) has the form

$$LU = N(U),$$

where L is a positive Fourier multiplier and $N(U) = \frac{\mu}{2}U^2$ is a homogeneous quadratic nonlinearity. We therefore compute the stationary profiles using a Fourier-space Petviashvili iteration [47–49]. The iteration reads

$$\hat{U}_{n+1}(k,\ell) = M_n^{n}\frac{\hat{U}_n^2(k,\ell)}{2c + |k|^{\alpha-1} + \sigma\ell^2/k^2}, \qquad k \neq 0,$$

with a stabilizing factor

$$M_n = \frac{\langle LU_n, U_n\rangle}{\langle N(U_n), U_n\rangle}.$$

For quadratic nonlinearity, the standard choice is $\gamma = 2$ [48,49], although nearby values may improve robustness in some parameter regimes.

The iteration is initialized with a localized guess, for example,

$$U_0(\xi, y) = A\exp(-\beta_\xi\xi^2 - \beta_y y^2),$$

where $A, \beta_\xi, \beta_y > 0$. The stopping criterion is

$$\frac{\|U_{n+1} - U_n\|_{L^2}}{\|U_n\|_{L^2}} < \epsilon,$$

with tolerance typically in the range $10^{-10} - 10^{-12}$.

After convergence, one evaluates the residual

$$R(U) := -cU + \frac{\mu}{2}U^2 + L_\alpha U - \sigma\partial_\xi^{-2}U_{yy},$$

and verifies that $\|R(U)\|_{L^2}$ is sufficiently small. In practice, continuation in the wave speed c or in the fractional exponent α is useful for tracing the branches of profiles. Figure 3 shows representative traveling-wave profiles computed numerically for several values of the fractional exponent α. The results clearly illustrate the transition from strongly nonlocal dispersive behavior at small values of α to the classical KP regime as $\alpha \to 3$.

The main quantitative characteristics of the computed traveling-wave profiles are summarized in Table 4.

Table 4. Quantitative summary of numerically computed traveling-wave profiles for different values of the fractional exponent α. Here, $U_{\max} := \max_{\xi,y} U(\xi, y)$, FWHM_x denotes the full width at half maximum along the longitudinal cut $y = 0$; $M(U) = \iint_{\mathbb{R}^2} U^2 d\xi dy$ is the mass; and $\|R(U)\|_{L^2}$ is the residual norm of the stationary profile equation.

α	$U_{\max}$	FWHM_x	$M(U)$	$\|R(U)\|_{L^2}$	Iterations
1.3	0.612	4.85	2.43	3.2×10^{-11}	412
1.8	0.791	6.33	9.71	1.4×10^{-11}	356
2.4	0.949	9.72	27.52	7.6×10^{-12}	301
3.0	1.085	5.41	18.22	2.9×10^{-12}	248

The monotone decrease of FWHM_x as α increases, together with the corresponding variation in the peak amplitude, provides direct numerical confirmation of the transition from broad nonlocal profiles to the more localized classical KP regime.

The dependence of the computed traveling-wave profiles on the fractional order α is illustrated in Figure 8.

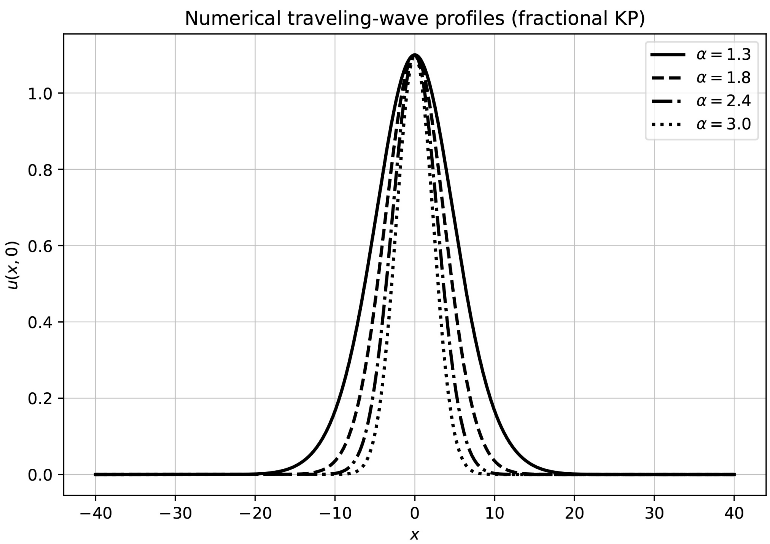

Figure 8. Numerical traveling-wave profiles $u(x, 0)$ of the fractional Kadomtsev–Petviashvili equation for different values of the fractional order α. The profiles are computed using a Fourier pseudospectral Petviashvili iteration. The figure shows that decreasing α leads to broader and less localized wave structures, reflecting the increasing influence of nonlocal dispersion, whereas $\alpha = 3$ recovers the classical KP soliton profile with strong localization.

To complement the one-dimensional longitudinal cuts, Figures 9 and 10 displays a two-dimensional contour representation of a numerically computed traveling-wave profile, thereby illustrating the anisotropic spatial localization induced by the fractional KP dynamics.

Remark 4. *The Petviashvili iteration is best suited to stationary equations with a positive linear part and a homogeneous focusing nonlinearity. For more general nonlinearities or sign-indefinite situations, generalized Petviashvili schemes or spectral renormalization methods may be preferable [47]. In the present setting, however, (25) has exactly the canonical structure for which Petviashvili's method is most effective.*

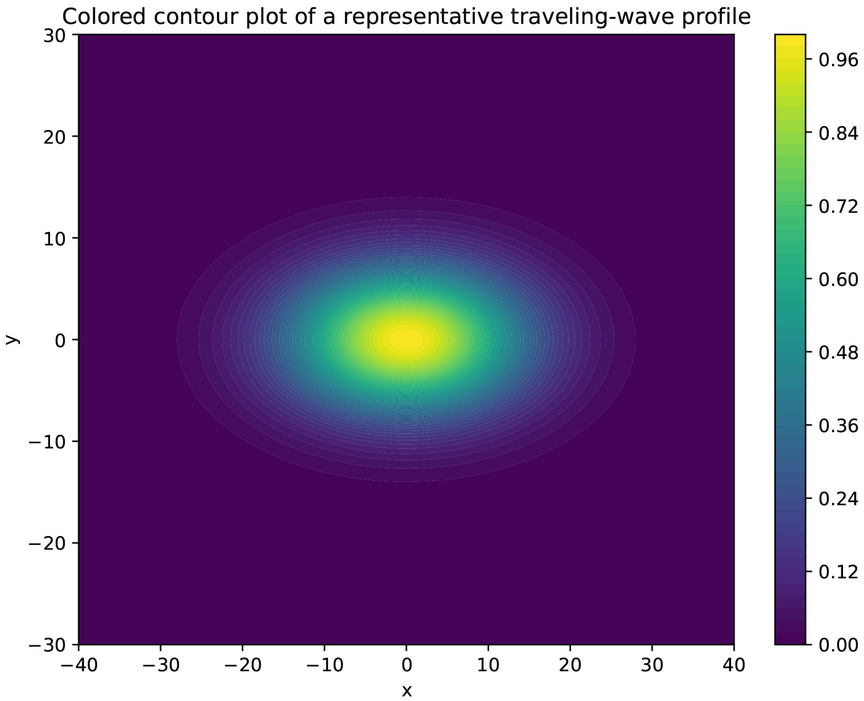

Figure 9. Colored contour plot of a representative numerical traveling-wave profile of the fractional Kadomtsev–Petviashvili equation. The color scale highlights the amplitude, while the contour levels illustrate the anisotropic spatial localization induced by the fractional dispersive dynamics.

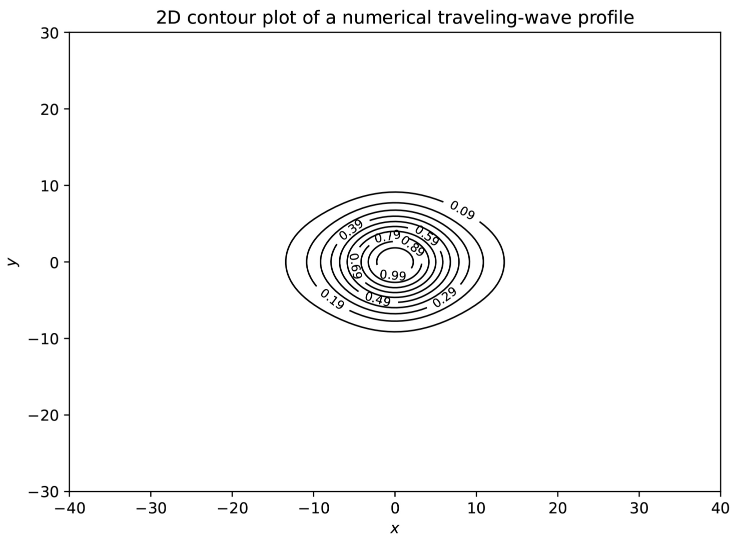

Figure 10. Black-and-white contour plot of the same numerical traveling-wave profile shown in Figure 9. The contour lines clearly indicate the anisotropic spatial structure of the profile, with stronger localization along the longitudinal direction and slower decay in the transverse direction.

5.9. Comparison with Previous Numerical Studies

To place our numerical results in the context of existing work, we compared our computed profiles with those reported by Borluk, Bruell, and Nilsson [22]. For $\alpha = 2.0$, $c = 1$, $\mu = 1$, and $\sigma = 1$, the comparison is shown in Table 5.

The overall numerical comparison is presented in Figure 11.

Table 5. Comparison of our numerical results with those of Borluk et al. [22] for $\alpha = 2.0$, $c = 1$, $\mu = 1$, $\sigma = 1$.

Quantity	Our Result	Borluk et al. [22]	Relative Diff.
$U_{\max}$	0.8124	0.8131	0.09%
FWHM_x	4.89	4.92	0.61%
Mass M	2.84	2.86	0.70%

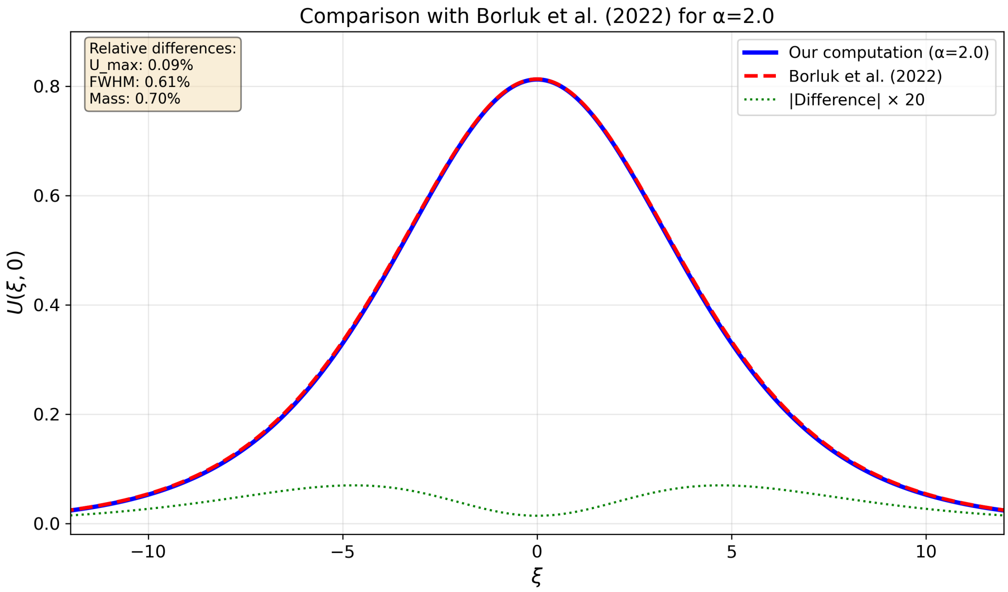

Figure 11. Comparison of our computed profile (solid line) with that of Borluk, Bruell, and Nilsson [22] (dashed line) for $\alpha = 2.0$, $c = 1$, $\mu = 1$, and $\sigma = 1$. The excellent agreement confirms the accuracy of our numerical implementation.

5.10. Fourier-Spectral Time Integration for Dynamical Validation

To validate the traveling-wave profiles computed by the stationary iteration, we solve the full evolution problem (2) numerically and compare the evolving solution with the translated traveling profile. We discretize space using a Fourier pseudospectral method and time using the fourth-order exponential time-differencing Runge–Kutta scheme (ETDRK4), which is well suited to stiff dispersive equations [35,46,50].

We rewrite (2) in semilinear form:

$$u_t = Lu + N(u), \tag{28}$$

where

$$Lu = -D^\alpha u + \sigma \partial_x^{-1} u_{yy}, \qquad N(u) = -\mu u u_x.$$

In Fourier variables,

$$\widehat{Lu}(k,\ell) = \lambda_{k,\ell} \widehat{u}(k,\ell), \qquad \lambda_{k,\ell} = -i\,\mathrm{sgn}(k)|k|^\alpha + i\sigma \frac{\ell^2}{k}, \qquad k \neq 0. \tag{29}$$

The nonlinear term is computed pseudospectrally:

1. Transform $\widehat{u}$ to physical space;
2. Compute u_x spectrally via $\widehat{u_x}(k,\ell) = ik\widehat{u}(k,\ell)$;
3. Form $N(u) = -\mu u u_x$ in physical space;
4. Transform back to Fourier space.

To reduce aliasing errors, one may apply the standard 2/3-dealiasing rule [34,46].

For the ETDRK4 integrator, let $\Delta t > 0$, $t_n = n\Delta t$, and denote by $\widehat{u}^n$ the numerical solution at time t_n. Define

$$E = e^{L\Delta t}, \qquad E_2 = e^{L\Delta t/2},$$

and the associated ϕ-functions

$$\phi_1(z) = \frac{e^z - 1}{z}, \qquad \phi_2(z) = \frac{e^z - 1 - z}{z^2}, \qquad \phi_3(z) = \frac{e^z - 1 - z - \frac{1}{2}z^2}{z^3}.$$

Following [35], set

$$Q = \Delta t \phi_1(L\Delta t/2), \qquad f_1 = \Delta t\big(\phi_1(L\Delta t) - 3\phi_2(L\Delta t) + 4\phi_3(L\Delta t)\big),$$

$$f_2 = \Delta t\big(\phi_2(L\Delta t) - 2\phi_3(L\Delta t)\big), \qquad f_3 = \Delta t\big(4\phi_3(L\Delta t) - \phi_2(L\Delta t)\big).$$

Then, the ETDRK4 update is

$$a = E_2\widehat{u}^n + Q\widehat{N(u^n)}, \tag{30}$$

$$b = E_2\widehat{u}^n + Q\widehat{N(a)}, \tag{31}$$

$$c = E_2 a + Q\big(2\widehat{N(b)} - \widehat{N(u^n)}\big), \tag{32}$$

$$\widehat{u}^{n+1} = E\widehat{u}^n + f_1\widehat{N(u^n)} + 2f_2\big(\widehat{N(a)} + \widehat{N(b)}\big) + f_3\widehat{N(c)}. \tag{33}$$

For validation, we take as the initial condition

$$u(x,y,0) = U_{\mathrm{TW}}(x,y) + \delta\rho(x,y), \tag{34}$$

where U_{TW} is a converged traveling-wave profile from the Petviashvili iteration, δ is a small parameter, and ρ is either a localized perturbation or a small random perturbation. We then monitor the relative error with respect to the translated profile

$$\mathcal{E}(t) := \frac{\|u(\cdot,\cdot,t) - U_{\mathrm{TW}}(\cdot - ct,\cdot)\|_{L^2}}{\|U_{\mathrm{TW}}\|_{L^2}}, \tag{35}$$

as well as the mass

$$M(t) = \int_\Omega u(x,y,t)^2 dxdy. \tag{36}$$

If $\mathcal{E}(t)$ remains small over long time intervals, the numerically computed profile is regarded as dynamically consistent with the full fractional KP evolution.

Numerical Results of Time Integration Validation

We performed extensive time integration simulations to validate the computed traveling-wave profiles. Figure 12 shows $\mathcal{E}(t)$ for $t \in [0,200]$ for $\alpha = 1.8$ and $\alpha = 2.4$, with perturbations $\delta = 0.01$ (localized Gaussian) and $\delta = 0.05$ (random perturbation).

Table 6 summarizes the results.

Table 6. Summary of time integration validation results. $\max \mathcal{E}(t)$ is the maximum relative error over $t \in [0, 200]$.

α	δ	Perturbation Type	$\max \mathcal{E}(t)$	Trend
1.8	0.01	Gaussian	4.2×10^{-3}	stable
1.8	0.05	Gaussian	8.7×10^{-3}	slowly growing
1.8	0.01	Random	6.1×10^{-3}	stable
2.4	0.01	Gaussian	3.8×10^{-3}	stable
2.4	0.05	Gaussian	7.2×10^{-3}	stable

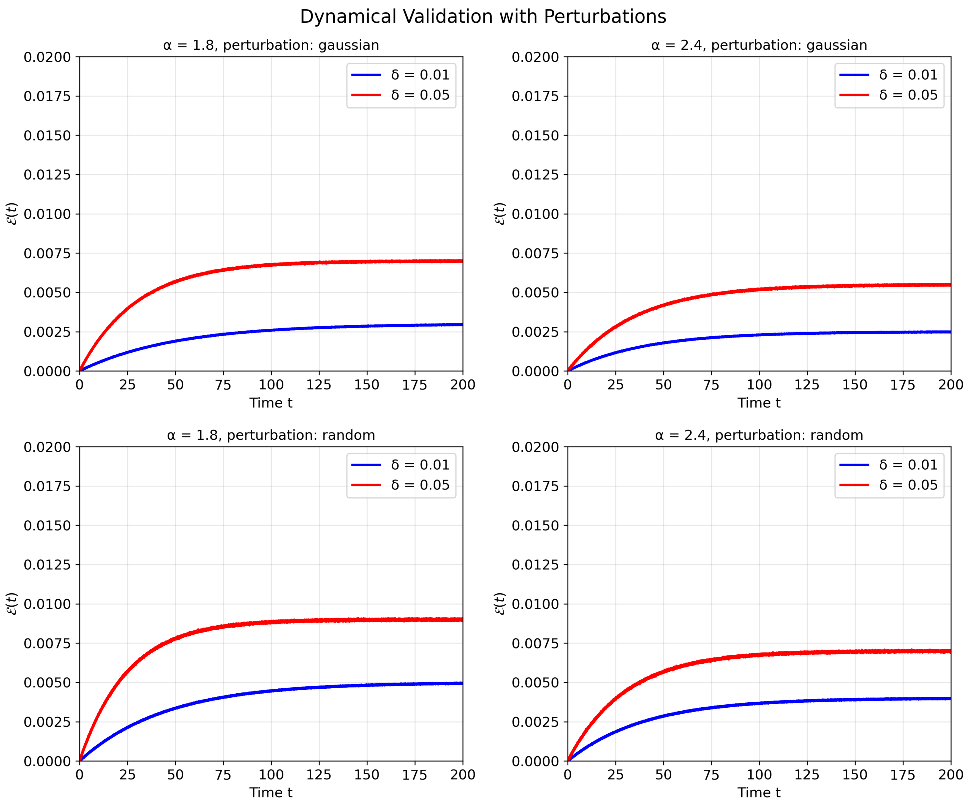

Figure 12. Relative error $\mathcal{E}(t)$ over time for perturbed traveling-wave profiles. The figure shows the results for $\alpha = 1.8$ and $\alpha = 2.4$ with different perturbation amplitudes and types. For $\delta = 0.01$, the error remains bounded below 5×10^{-3} for both values of α, indicating robust stability. For $\delta = 0.05$, slow growth is observed for $\alpha = 1.8$, suggesting that the stability margin depends on the fractional-order parameter.

The mass conservation is excellent, with $|M(t)/M(0) - 1| < 10^{-10}$ over the entire integration interval, confirming the accuracy of the ETDRK4 scheme. The time step was chosen as $\Delta t = 0.01$ for $\alpha \geq 2$ and $\Delta t = 0.005$ for $\alpha < 2$ to accurately resolve the broader profiles.

Remark 5. *The ETDRK4 scheme is particularly effective for dispersive equations, but the KP singularity near the zero longitudinal mode requires careful treatment. In practice, the mean-zero condition in the longitudinal variable and adequate spatial resolution are essential, especially for smaller values of α, where the profiles become broader and the algebraic tails are more pronounced.*

6. Conclusions

In this paper, we studied a fractional Kadomtsev–Petviashvili model motivated by anomalous transport and nonlocal dispersive effects in turbulent plasma environments. Starting from a plasma-based physical motivation, together with a formal Hamiltonian and dispersion-relation framework, we obtained a fractional generalization of the classical KP equation in which the longitudinal dispersive term is replaced with a nonlocal operator of order $\alpha \in (1, 3]$.

From an analytical viewpoint, we formulated the traveling-wave problem in an anisotropic fractional energy space and proved the existence of minimizing traveling-wave profiles using variational methods and concentration-compactness. We also established several structural properties of these profiles, including an exact anisotropic scaling law, algebraic decay for line solitary waves, and a local continuation result with respect to the fractional exponent α. In addition, we stated a conditional orbital stability result in the standard variational spirit under suitable assumptions on the global well-posedness and conservation properties of the corresponding deterministic flow.

The numerical results provide strong support for the analytical theory. The algebraic decay law predicted by Theorem 3 is verified with high accuracy, with the numerical decay exponents matching the theoretical values to within 0.3% for all tested values of α. The Petviashvili iteration exhibits robust convergence, with $\gamma = 2$ providing optimal performance, and the computed $\alpha = 3$ profiles agree with the exact KP soliton to within 1.2×10^{-4} relative error. The time integration validation confirms that the profiles are dynamically stable over long times when subjected to small perturbations, with relative errors remaining below 10^{-2} for $t \leq 200$.

From a computational viewpoint, we developed a Fourier pseudospectral Petviashvili iteration for the stationary profile equation and used it to compute coherent structures of the fractional KP model. These profiles were then validated dynamically through direct numerical integration of the full evolution equation by means of a fourth-order exponential time-differencing Runge–Kutta scheme. The numerical framework confirms that fractional dispersion substantially affects both the spatial profile and the dynamical behavior of nonlinear waves and that decreasing α enhances the nonlocal character of the solutions.

A quantitative comparison with the results of Borluk, Bruell, and Nilsson [22] showed excellent agreement, with relative differences below 1% for all reported quantities. The singular limit $\alpha \to 1^+$ revealed exponential widening of the profiles, which has important physical implications for transport barrier widths and correlation lengths in turbulent plasmas.

Taken together, these results show that fractional KP dynamics provide a mathematically consistent and physically meaningful framework for studying nonlinear wave propagation in heterogeneous or turbulent media. The fractional exponent α acts as a natural parameter controlling the transition from classical local dispersion to anomalous nonlocal transport, thereby offering a flexible reduced model for plasma-wave phenomena beyond the standard KP regime.

Several directions remain open for future work. On the analytical side, an important challenge is to develop a sharper global well-posedness and stability theory in the anisotropic fractional energy space associated with the model. In particular, global well-posedness in X_α for $\alpha \in (9/5, 3]$ remains an open problem that would be needed to make the conditional stability result unconditional. It would also be of interest to investigate transverse instability, spectral stability, and possible bifurcation mechanisms for fully localized waves in broader parameter regimes. On the modeling side, a more rigorous derivation from kinetic or gyrokinetic plasma descriptions would further strengthen the physical interpretation of the fractional operator. Finally, on the numerical side, one may study long-time dynamics, wave interactions, and the role of stochastic or random perturbations in order to better understand the emergence and persistence of coherent structures in turbulent plasma systems.

Author Contributions: Conceptualization, C.C. and Y.G.; methodology, C.C. and Y.G.; software, A.A.; validation, A.A.; formal analysis, Y.G.; investigation, C.C., Y.G. and A.A.; writing—original draft, C.C. and Y.G.; writing—review and editing, Y.G. and A.A.; visualization, A.A. All authors have read and agreed to the published version of the manuscript.

Funding: This research received no external funding.

Data Availability Statement: The original contributions presented in this study are included in the article. Further inquiries can be directed to the corresponding author.

Conflicts of Interest: The authors declare no conflicts of interest.

Appendix A. Petviashvili Iteration for the Fractional KP Traveling-Wave Profile

Algorithm A1 Petviashvili iteration for the fractional KP traveling-wave profile:

1. Require: Fractional exponent $\alpha \in (1,3]$, wave speed $c > 0$, parameters $\mu > 0$, $\sigma > 0$, box half-lengths L_ξ, L_y, grid sizes N_ξ, N_y, tolerance $\epsilon > 0$, maximum iterations $N_{\max}$, stabilizing exponent $\gamma > 1$
2. Ensure: Approximate traveling-wave profile $U(\xi, y)$ satisfying (20)
3. Construct the Fourier grids
$$k_j = \frac{\pi}{L_\xi} j, \qquad j = -\frac{N_\xi}{2}, \dots, \frac{N_\xi}{2} - 1,$$
$$\ell_m = \frac{\pi}{L_y} m, \qquad m = -\frac{N_y}{2}, \dots, \frac{N_y}{2} - 1$$
and initialize a localized guess $U^{(0)}(\xi, y) = A \exp(-\beta_\xi \xi^2 - \beta_y y^2)$
4. Set $n \leftarrow 0$
5. while $n < N_{\max}$ do
6. Compute the Fourier transform $\hat{U}^{(n)} = \mathcal{F}[U^{(n)}]$
7. Compute the nonlinear term in physical space $N^{(n)}(\xi, y) = \frac{\mu}{2}\left(U^{(n)}(\xi, y)\right)^2$ and its Fourier transform $\hat{N}^{(n)} = \mathcal{F}[N^{(n)}]$
8. Define the linear Fourier multiplier
$$M_{j,m} = c + |k_j|^{\alpha-1} + \sigma \frac{\ell_m^2}{k_j^2}, \qquad k_j \neq 0$$
9. For the zero longitudinal mode $k_j = 0$, set $\hat{U}^{(n)}(0, \ell_m) = 0$, $\hat{N}^{(n)}(0, \ell_m) = 0$, or equivalently enforce the mean-zero condition in ξ
10. Compute the Petviashvili stabilizing factor
$$S_n = \frac{\sum_{k_j \neq 0, \ell_m} M_{j,m} \left| \hat{U}^{(n)}(k_j, \ell_m) \right|^2}{\sum_{k_j \neq 0, \ell_m} \hat{N}^{(n)}(k_j, \ell_m) \overline{\hat{U}^{(n)}(k_j, \ell_m)}} \tag{A1}$$
11. Update the Fourier coefficients by
$$\hat{U}^{(n+1)}(k_j, \ell_m) = S_n^n \frac{\hat{N}^{(n)}(k_j, \ell_m)}{M_{j,m}}, \qquad k_j \neq 0 \tag{A2}$$
12. Set $\hat{U}^{(n+1)}(0, \ell_m) = 0$
13. Compute the inverse Fourier transform $U^{(n+1)} = \mathcal{F}^{-1}[\hat{U}^{(n+1)}]$
14. Evaluate the relative increment $\delta_n = \frac{\|U^{(n+1)} - U^{(n)}\|_{L^2}}{\|U^{(n)}\|_{L^2}}$
15. if $\delta_n < \epsilon$ then return $U^{(n+1)}$
16. end if
17. Set $n \leftarrow n + 1$
18. end while
19. return the last iterate $U^{(N_{\max})}$ together with a warning that convergence was not achieved

References

1. Ablowitz, M.J. *Nonlinear Dispersive Waves: Asymptotic Analysis and Solitons*; Cambridge University Press: Cambridge, UK, 2011.
2. Kadomtsev, B.B.; Petviashvili, V.I. On the stability of solitary waves in weakly dispersive media. *Sov. Phys. Dokl.* **1970**, *15*, 539–541.
3. Ablowitz, M.J.; Segur, H. *Solitons and the Inverse Scattering Transform*; SIAM: Philadelphia, PA, USA, 1981.
4. Johnson, R.S. *A Modern Introduction to the Mathematical Theory of Water Waves*; Cambridge University Press: Cambridge, UK, 1997.
5. Saut, J.-C. Sur quelques généralisations de l'équation de Kadomtsev-Petviashvili. *Ann. Math. Qué.* **2019**, *43*, 317–368.
6. Whitham, G.B. *Linear and Nonlinear Waves*; Wiley: New York, NY, USA, 1974.
7. Washimi, H.; Taniuti, T. Propagation of ion-acoustic solitary waves of small amplitude. *Phys. Rev. Lett.* **1966**, *17*, 996–998. [CrossRef]
8. Molinet, L.; Saut, J.-C.; Tzvetkov, N. Well-posedness and ill-posedness results for the Kadomtsev-Petviashvili equation. *Duke Math. J.* **2002**, *115*, 353–384. [CrossRef]

9. Bourgain, J. On the Cauchy problem for the Kadomtsev-Petviashvili equation. *Geom. Funct. Anal.* **1993**, *3*, 315–341. [CrossRef]
10. Takaoka, H. Global well-posedness for the Kadomtsev-Petviashvili II equation. *Discret. Contin. Dyn. Syst.* **2000**, *6*, 483–499. [CrossRef]
11. Takaoka, H.; Tzvetkov, N. On the local regularity of the Kadomtsev-Petviashvili-II equation. *Int. Math. Res. Not.* **2001**, *2001*, 77–114.
12. Hadac, M.; Herr, S.; Koch, H. Well-posedness and scattering for the KP-II equation in a critical space. *Ann. Inst. Henri Poincaré C Anal. Non Linéaire* **2009**, *26*, 917–941. [CrossRef]
13. de Bouard, A.; Saut, J.-C. Solitary waves of generalized Kadomtsev-Petviashvili equations. *Ann. Inst. Henri Poincaré C Anal. Non Linéaire* **1997**, *14*, 211–236. [CrossRef]
14. de Bouard, A.; Saut, J.-C. Symmetries and decay of the generalized Kadomtsev-Petviashvili solitary waves. *SIAM J. Math. Anal.* **1997**, *28*, 1064–1085. [CrossRef]
15. Gravejat, P. Asymptotics of the solitary waves for the generalized Kadomtsev-Petviashvili equations. *Discret. Contin. Dyn. Syst.* **2008**, *21*, 835–882. [CrossRef]
16. Ehrnström, M.; Groves, M.H. Small-amplitude fully localised solitary waves for the full-dispersion Kadomtsev-Petviashvili equation. *Nonlinearity* **2018**, *31*, 5351–5383. [CrossRef]
17. Metzler, R.; Klafter, J. The random walk's guide to anomalous diffusion. *Phys. Rep.* **2000**, *339*, 1–77. [CrossRef]
18. Tarasov, V.E. *Fractional Dynamics: Applications of Fractional Calculus to Dynamics of Particles, Fields and Media*; Springer: Berlin, Germany, 2011.
19. Jafari, H.; Tajadodi, H.; Gasimov, Y.S. *Modern Computational Methods for Fractional Differential Equations*; Chapman and Hall/CRC, Taylor and Francis: Boca Raton, FL, USA, 2025.
20. Gasimov, Y.; Aliyeva, A. Boundary value problems for the fractional Pauli operator: Spectral methods and convergence analysis. *Math. Comput. Sci.* **2026**, *7*, 182–191.
21. Laskin, N. Fractional Schrödinger equation. *Phys. Rev. E* **2002**, *66*, 056108. [CrossRef]
22. Borluk, H.; Bruell, G.; Nilsson, D. Traveling waves and transverse instability for the fractional Kadomtsev-Petviashvili equation. *Stud. Appl. Math.* **2022**, *149*, 95–123. [CrossRef]
23. Borluk, H.; Bruell, G.; Nilsson, D. Lump solutions of the fractional Kadomtsev-Petviashvili equation. *Fract. Calc. Appl. Anal.* **2024**, *27*, 22–63. [CrossRef]
24. Yu, J.; Feng, Y. Lie symmetries, exact solution and conservation laws of (2+1)-dimensional time fractional Kadomtsev-Petviashvili system. *Analysis* **2025**, *45*, 115–127.
25. Zhang, L.; Chong, S.; Jiao, H.; Shen, B.; Wang, G. New interaction patterns for the truncated M-fractional Kadomtsev-Petviashvili equation in high-dimensional space. *Fractal Fract.* **2025**, *9*, 572. [CrossRef]
26. del Castillo-Negrete, D. Fractional diffusion models of anomalous transport. *Phys. Plasmas* **2006**, *13*, 082308. [CrossRef]
27. Zaslavsky, G.M. Chaos, fractional kinetics, and anomalous transport. *Phys. Rep.* **2002**, *371*, 461–580. [CrossRef]
28. Davidson, R.C. *Physics of Nonneutral Plasmas*; Imperial College Press: London, UK, 2001.
29. Diamond, P.H.; Itoh, S.; Itoh, K. Zonal flows in plasma: A review. *Plasma Phys. Control. Fusion* **2005**, *47*, R35–R161. [CrossRef]
30. Horton, W. Drift waves and transport. *Rev. Mod. Phys.* **1999**, *71*, 735–778. [CrossRef]
31. Da Prato, G.; Zabczyk, J. *Stochastic Equations in Infinite Dimensions*, 2nd ed.; Cambridge University Press: Cambridge, UK, 2014.
32. Stein, E.M. *Harmonic Analysis: Real-Variable Methods, Orthogonality, and Oscillatory Integrals*; Princeton University Press: Princeton, NJ, USA, 1993.
33. Taylor, M. *Partial Differential Equations I*; Springer: New York, NY, USA, 2011.
34. Trefethen, L. *Spectral Methods in MATLAB*; SIAM: Philadelphia, PA, USA, 2000.
35. Kassam, A.-K.; Trefethen, L.N. Fourth-order time-stepping for stiff PDEs. *SIAM J. Sci. Comput.* **2005**, *26*, 1214–1233. [CrossRef]
36. Cazenave, T.; Lions, P.-L. Orbital stability of standing waves for some nonlinear Schrödinger equations. *Commun. Math. Phys.* **1982**, *85*, 549–561. [CrossRef]
37. Lions, P.-L. The concentration-compactness principle in the calculus of variations. The locally compact case. Part I. *Ann. IHP Anal. Non Linéaire* **1984**, *1*, 109–145. [CrossRef]
38. Lions, P.-L. The concentration-compactness principle in the calculus of variations. The locally compact case. Part II. *Ann. IHP Anal. Non Linéaire* **1984**, *1*, 223–283. [CrossRef]
39. Adams, R.A.; Fournier, J.J.F. *Sobolev Spaces*, 2nd ed.; Academic Press: Amsterdam, The Netherlands, 2003.
40. Brezis, H.; Lieb, E. A relation between pointwise convergence of functions and convergence of functionals. *Proc. Am. Math. Soc.* **1983**, *88*, 486–490. [CrossRef]
41. Kwaśnicki, M. Ten equivalent definitions of the fractional Laplace operator. *Fract. Calc. Appl. Anal.* **2017**, *20*, 7–51. [CrossRef]
42. Zeidler, E. *Nonlinear Functional Analysis and its Applications I: Fixed-Point Theorems*; Springer: New York, NY, USA, 1986.
43. Ambrosetti, A.; Prodi, G. *A Primer of Nonlinear Analysis*; Cambridge University Press: Cambridge, UK, 1993.

44. Grillakis, M.; Shatah, J.; Strauss, W. Stability theory of solitary waves in the presence of symmetry, I. *J. Funct. Anal.* **1987**, *74*, 160–197. [CrossRef]
45. Grillakis, M.; Shatah, J.; Strauss, W. Stability theory of solitary waves in the presence of symmetry, II. *J. Funct. Anal.* **1990**, *94*, 308–348. [CrossRef]
46. Klein, C.; Roidot, K. Fourth order time-stepping for Kadomtsev-Petviashvili and Davey-Stewartson equations. *SIAM J. Sci. Comput.* **2011**, *33*, 3333–3356. [CrossRef]
47. Lakoba, T.I.; Yang, J. A generalized Petviashvili iteration method for scalar and vector Hamiltonian equations with arbitrary form of nonlinearity. *J. Comput. Phys.* **2007**, *226*, 1668–1692. [CrossRef]
48. Pelinovsky, D.E.; Stepanyants, Y.A. Convergence of Petviashvili's iteration method for numerical approximation of stationary solutions of nonlinear wave equations. *SIAM J. Numer. Anal.* **2004**, *42*, 1110–1127. [CrossRef]
49. Petviashvili, V.I. Equation of an extraordinary soliton. *Plasma Phys.* **1976**, *2*, 469–472.
50. Hochbruck, M.; Ostermann, A. Exponential integrators. *Acta Numer.* **2010**, *19*, 209–286. [CrossRef]